Gut Microbiota Orchestrates Energy Homeostasis During Cold

Claire Chevalier[1,2*], Ozren Stojanović[1,2*], Didier J. Colin[3], Nicolas Suarez-Zamorano[1,2], Valentina Tarallo[1,2], Christelle Veyrat-Durebex[1,2], Dorothée Rigo[1,2], Salvatore Fabbiano[1,2], Ana Stevanović[1,2], Stefanie Hagemann[4] Xavier Montet[5], Yann Seimbille[3], Nicola Zamboni[6], Siegfried Hapfelmeier[4], Mirko Trajkovski[1,2,7,†]

[1]University of Geneva, Medical Faculty, Department of Cell Physiology and Metabolism, Centre Médical Universitaire (CMU), 1211 Geneva 4, Switzerland

[2]University of Geneva, Diabetes Centre, Faculty of Medicine, 1211 Geneva, Switzerland

[3]Geneva University Hospital, Centre for BioMedical Imaging (CIBM), 1211 Geneva, Switzerland

[4]University of Bern, Institute for Infectious Diseases, 3010 Bern, Switzerland

[5]Geneva University Hospital, Division of radiology, 1211 Geneva, Switzerland

[6]Swiss Federal Institute of Technology (ETH) Zurich, Institute for Molecular Systems Biology, 8093 Zurich, Switzerland

[7]University College London (UCL), Division of Biosciences, Institute of Structural and Molecular Biology, WC1E 6BT, London, UK

[*]Co-first authors

[†]Correspondence:
Mirko Trajkovski
University of Geneva, Medical Faculty,
Department of Cell Physiology and Metabolism,
Centre Médical Universitaire (CMU),
Rue Michel Servet 1, 1211 Geneva 4, Switzerland
Tel.: +41 (0)22 37 95 256
Fax : +41 (0)22 37 95 260
E-mail: Mirko.Trajkovski@unige.ch

Summary

Microbial functions in the host physiology are a result of the microbiota-host co-evolution. We show that cold exposure leads to marked shift of the microbiota composition, referred to as cold microbiota. Transplantation of the cold microbiota to germ-free mice is sufficient to increase insulin sensitivity of the host, and enable tolerance to cold partly by promoting the white fat browning, leading to increased energy expenditure and fat loss. During prolonged cold however, the body weight loss is attenuated, caused by adaptive mechanisms maximising caloric uptake and increasing intestinal, villi and microvilli lengths. This increased absorptive surface is transferable with the cold microbiota leading to altered intestinal gene expression promoting tissue remodelling and suppression of apoptosis - effect diminished by co-transplanting the most cold-downregulated strain *Akkermansia muciniphila* during the cold microbiota transfer. Our results demonstrate the microbiota as a key factor orchestrating the overall energy homeostasis during increased demand.

Introduction

Food intake, energy expenditure (EE) and body adiposity are homeostatically regulated, and malfunctions of this balance can cause obesity (Murphy and Bloom, 2006) (Farooqi and O'Rahilly, 2005). Mammalian white adipose tissue (WAT) is an important regulator of the whole body homeostasis that stores energy in form of triglycerides (TGs). The brown adipose tissue (BAT) catabolises lipids to produce heat, function mediated by the tissue-specific uncoupling protein 1 (Ucp1) abundantly present in the BAT mitochondria. BAT differentiation can be induced by prolonged cold exposure and beta-adrenergic

stimulation which leads to elevated intracellular cyclic AMP (Cannon and Nedergaard, 2004) (Young et al., 1984). The BAT is present at distinct anatomical sites, including the interscapular, perirenal and axillary depots. Brown fat cells also emerge in subcutaneous WAT (SAT) (known as “beige” cells) in response to cold or exercise (Cousin et al., 1992) (Guerra et al., 2001), a process referred to as WAT browning. Loss of BAT function is linked to obesity and metabolic diseases (Lowell et al., 1993). Promotion of increased BAT development on the other hand, increases EE without causing dysfunction in other tissues and is associated with a lean and healthy phenotype (Ghorbani et al., 1997; Guerra et al., 1998; Kopecky et al., 1995), suggesting the manipulation of the fat stores as an important therapeutic objective.

The gastrointestinal tract is the body's largest endocrine organ that releases a number of regulatory peptide hormones that influence many physiological processes (Badman and Flier, 2005). The intestinal epithelium undergoes rapid self-renewal fueled by multipotent Lgr5-expressing stem cells located in the crypts of Lieberkuhn and is terminated by apoptosis/exfoliation of terminally differentiated cells at the tips of small intestinal villi (Sato et al., 2009). At the apical surface, the epithelial cells have microvilli that further substantially increase the absorptive area and mediate the secretory functions. The intestinal microbiota co-develops with the host, and its composition is influenced by several physiological changes (Koren et al., 2012; Liou et al., 2013; Ridaura et al., 2013). The colonization starts immediately after birth and is initially defined by the type of delivery and early feeding. After one year of age, the intestinal microbiota is already shaped and stabilized, but continues to be influenced by environmental factors including

diet (Sekirov et al., 2010). A wide range of pathologies have been associated with alterations of the gut microbial composition (e.g.: asthma, arthritis, autism or obesity) (Sommer and Backhed, 2013). The intestinal microbiota can also influence the whole-body metabolism by affecting energy balance (Backhed et al., 2004) (Chou et al., 2008) (Turnbaugh et al., 2006) (Koren et al., 2012) (Ridaura et al., 2013). The mechanisms and the nature of the phenotypic and morphological changes that regulate the energy homeostasis of the new host following microbiota transplantation remain poorly understood. Here we show that the microbiota remodelling is an important contributor of the beige fat induction during cold, and a key factor that promotes energy uptake by increasing the intestinal absorptive area, thus orchestrating the overall energy homeostasis during increased energy demand.

Results

Cold Exposure Changes the Gut Microbiota Composition. Short-term cold exposure for up to ten days leads to increased EE relative to the energy uptake, and suppresses BW and white fat mass gain (Figure S1A–F) (Wu et al., 2012; Wu et al., 2013). To investigate the importance of the acutely consumed food and caloric harvest during cold exposure, we restricted the food access during the initial 8 hours (hr) of cold exposure, or depleted the intestinal microbiota using broad range antibiotics (Abx) administered in the drinking water. The higher fecal caloric content after complete microbiota depletion was confirmed using bomb calorimetry (Figure S1G), and was consistent with previous reports (El Kaoutari et al., 2013), suggesting lower energy harvest from the food. Restricting the food access during acute cold exposure led to decreased body temperature

(Figure 1A, B) compared to ad libitum fed control mice, and to marked drop in the blood glucose and BW at cold (Figure S1H–J). The decreased tolerance to cold and lowered blood glucose levels were also evident in the Abx mice and the changes were relatively stable during short and long-term microbiota depletion up to four weeks of treatment (Figure 1C–E, S1K–R), despite the stable food intake and slightly increased water consumption (Figure S1S,T). These data suggest that the energy harvest during acute cold contributes to maintaining the body temperature, and that the intestinal microbiota is supporting this process.

We observed that over time, the overall fat loss was attenuated despite the stable food intake and EE (Figure S1A–F), suggesting compensatory mechanisms that enable increased caloric harvest from the consumed food. To investigate whether this prolonged cold exposure causes changes in the intestinal microbiota, we collected feces at days 0, 11 and 31 and cecum post–mortem of cold-exposed mice and RT controls. Profiling of the microbiota composition by 16S rRNA gene sequencing, followed by principal coordinates analysis (PCoA) based on weighted UniFrac distance showed major alterations of the microbiota content both in cecum, and feces samples of cold exposed animals (Figure S2A, B, Figure 1F). As expected, Firmicutes was the richest phylum in all samples (on average 69.10%) (Figure 1I, J). Bacteroidetes was the most abundant phylum **(**on average 63.50%) in all samples except the cold exposed day 31 samples (Figure S2C–E). We observed differences in operational taxonomic units (OTUs) abundance at phylum-level in Bacteroidetes, Firmicutes, Verrucomicrobia, Deferribacteres, Cyanobacteria and Actinobacteria; and differences in OTU numbers at

phylum-level in all the above plus Deferribacteres based on factor summary barchart. Individual species, or family based hierarchical clustering using the average-neighbor method confirmed the major shift of the microbiota composition, and showed clustering of the samples from the cold exposed versus the room temperature (RT) groups in both feces and cecum samples (Figure 1G, S2D,F, S3A,B). Comparison of phylum level proportional abundance in feces showed shifts in proportions (Figure 1H, S2C), especially in the ratio Firmicutes/Bacteroidetes where Firmicutes abundance (from 18.6% in RT up to 60.5% under cold) increased over Bacteroidetes (from 72.6% in RT to 35.2% under cold). The Verrucomicrobia phylum was almost absent from both feces and cecum after the cold exposure (from 12.5% for the RT to 0.003% for the cold in cecum) (Figure 1H, S2C, E). Interestingly, similar shifts, although less pronounced, are associated with genetic and high fat diet induced obesity (Turnbaugh et al., 2006). The shifts in phylum abundance correlated with the richness of the species present in them. Firmicutes phylum increased its richness in feces up to 78.1% under cold exposure (compared to 65% in RT) and Bacteroidetes decreased it to 18.8% (compared to 29.7% in RT) (Figure 1I, J), without changing the overall bacterial diversity based on the Shannon diversity index (Figure S3C, D). From the 3864 OTUs detected, using Welch t-test done across the two groups of samples using the abundance metrics, 252 OTUs (within 44 families) were significantly different ($p < 0.05$). Of the selected families, there were mixed responses in Firmicutes, Proteobacteria and Bacteroidetes, however those within Actinobacteria, Verrucomicrobia and Tenericutes were less abundant in the cold samples, while RT samples were less abundant in Deferribacteres (Figure 1K). When looking at the most significantly changed OTUs using analysis of variance, *Akkermansia muciniphila* and

S24-7 family were among the top 9 most shifted bacteria (Figure S3G, H). Verrucomicrobia phylum was represented by 8 different OTUs, all part of the same species: *Akkermansia muciniphila*, which we found highly decreased with cold exposure (Figure S3E, F). The changes in the major bacterial phyla were confirmed by qPCR in the sequenced, as well as in independent sets of SPF and conventional animals (Figure S3I–L). Together these results demonstrate a major shift in lower gut microbiota in response to cold exposure.

Cold Microbiota Transplantation Increases Insulin Sensitivity. To investigate the importance of the microbiota changes during cold, we transplanted the microbiota from 30 days cold-exposed, or control RT mice to GF mice by co-habitation, and again confirmed the shifts in the donors and the recipient mice (Figure S3K, L). As expected, cold exposure of donor mice led to a marked increase in the insulin sensitivity (Figure 2A). Strikingly, cold microbiota transplanted mice also showed increased sensitivity to insulin (Figure 2B), suggesting that cold microbiota alone is sufficient to transfer part of this phenotype. The increased insulin sensitivity was further investigated using hyperinsulinemic-euglycemic clamp in awake and unrestrained mice. Cold mice showed a marked increase in the glucose infusion rates (GIR) needed to maintain the clamped glucose levels, and an increase in the stimulated glucose disappearance (Rd) levels (Figure 2C, D, S4A). To investigate the peripheral glucose uptake, we co-administered 2-[^{14}C]deoxyglucose (2[^{14}C]DG) during the clamp. While no changes were observed in the glucose uptake from interscapular BAT (iBAT), brain, soleus or quadriceps muscle, there was a large increase in the uptake from inguinal subcutaneous and perigonadal

(epididymal in males) visceral depots of the WAT (ingSAT and pgVAT, respectively) (Figure 2E). These observations were further corroborated in glucose stimulated and basal conditions (Figure 2F, G), which in addition showed increased glucose uptake in iBAT. Interestingly, the cold microbiota transferred the fat specific glucose disposal phenotype to the transplanted mice as measured by 2[^{14}C]DG uptake (Figure 2H), and by positron emission tomography-computed tomography (microPET-CT). Specifically, both ingSAT and pgVAT, but not quadriceps muscle, showed increased [^{18}F]fluorodeoxyglucose ([^{18}F]FDG) uptake in the cold transplanted mice (Figure 2I–K), and had decreased ingSAT and pgVAT volumes and weights (Figure 3A–F, S4B). Hounsfield unit (HU) analysis of the microCT scans revealed that cold microbiota transplanted mice had higher ingSAT and pgVAT density compared to the controls (Figure 3G, H). Together, these data suggest that the cold microbiota contributes to the increased insulin sensitivity observed during cold exposure, and leads to decreased total fat coupled with increased fat density.

Cold Microbiota Promotes Browning, Energy Expenditure and Cold Tolerance. To investigate whether the higher density and the decreased fat amount (Figure 3A–H) are originating from the differences in the adipocyte volume, we measured the adipocyte size distribution using high content imaging. Cold transplanted mice had increased number of small, and decreased number of large adipocytes in the ingSAT and pgVAT depots (Figure 3I–L). The adipose depots excised from the cold transplanted animals were darker in appearance. All these phenotypic events are characteristic features of mature beige adipocytes. Therefore, we investigated whether cold microbiota could affect the

browning of the white fat depots, and found that cold transplanted mice had marked increase in the brown fat specific markers in the ingSAT, and surprisingly, also in the pgVAT depots (Figure 3M, O). The increased browning of ingSAT was consistent with the increased Ucp1-positive cells in the cold transplanted mice (Figure 3N). There was a tendency bordering significance towards increased brown fat marker expression in the interscapular BAT (iBAT) depots of the cold transplanted mice, albeit at smaller scale compared to ingSAT and pgVAT (Figure 3P). Together, these data suggest that cold microbiota alone can be sufficient to induce beige/brown fat formation primarily in the ingSAT and pgVAT, and to a smaller magnitude in the iBAT depots. The increased browning was consistent with the enhanced resting EE (REE) of the cold transplanted mice (Figure 3Q), suggesting increased energy dissipation. To further investigate it's functional relevance, we exposed the cold transplanted mice to acute cold, and monitored the internal body temperature, as well as ventrally or dorsally, indicative of the temperature emitted from ingSAT, or iBAT depots. The rectal temperature measurements showed that the RT transplanted mice had decreased body temperature following 4 hr of cold exposure, but only a mild temperature drop was detected in the cold transplanted mice (Figure 4A, B). Accordingly, the infrared imaging and quantification of the different regions (Figure 4C) demonstrated that cold microbiota transplanted mice are fully resistant to cold stress as shown by the eye temperature measurements, representative of the internal body temperature (Figure 4D, G). Analysis of the dorsal and ventral infrared images showed that the inguinal and the interscapular region contribute to the overall tolerance to cold. Specifically, while the differences in dorsal temperatures were transient between the groups (Figure 4E, H), the maximal ventral heat differences

remained constant also after 12 hr of cold exposure (Figure 4F, I). These data suggest a mechanistic explanation for the increased insulin sensitivity, and demonstrate that the cold microbiota alone is sufficient to induce tolerance to cold, increased EE and lower fat content, and that this effect is partially mediated by the browning of the white fat depots.

Cold Exposed, and Cold Microbiota Transplanted Mice Have Increased Intestinal Absorptive Surface. Next, we monitored short-chain fatty acids (SCFAs), volatile compounds and organic acids associated with gut flora activity using mass spectrometry (Table S1 and S2). In lipid cecal extracts butyrate, the primary energy source in colon and the most abundant SCFA (Ferreyra et al., 2014), was markedly decreased in antibiotic treated mice and, accordingly, increased upon gut flora transplantation (Table S2). Similarly, succinate, a frequent product of primary fermenters that is utilized by butyrogenic bacteria (Wichmann et al., 2013), was decreased in absence of gut flora. We observed increase of propionate, butyrate, lactate and succinate in cold transplanted mice (Table S2). These results could indicate increased fermentation activity of cold over RT microbiota, associated with increased energy harvest.

As mentioned, during long-term cold exposure and after the initial weight loss, the BW stabilizes despite the constantly increased EE rates and heat production, suggesting increased nutrient absorption from the relatively stable food intake. Oral glucose tolerance tests (OGTT) in cold exposed mice with or without microbiota depletion showed an elevated glucose peak following glucose gavage compared to RT controls (Figure 5A, S4C–G) after 15 min, but also faster clearance, consistent with the increased

insulin sensitivity (Figure S4H). Interestingly, no differences were observed in the initial glucose peak when glucose was administered intraperitoneally (Figure S4I). This suggests that orally administered glucose is rapidly taken up in cold exposed and in microbiota depleted mice. The rapid glucose uptake was observed also in the cold transplanted mice, which showed increased glucose peaks 7.5 and 15 min after glucose gavage (Figure 5B), and no changes in the insulin release compared to the RT transplanted (Figure S4J). This was consistent with increased triglyceride uptake and non-esterified fatty acid levels in the cold transplanted mice (Figure 5C, D), suggesting increased total energy harvest levels following oral gavage in the cold transplanted mice. To confirm that cold exposure leads to increase in the calorie uptake, we measured the fecal caloric content using bomb calorimetry and calculated the total energy uptake. Cold exposed mice showed increased caloric uptake, and this was phenocopied in the cold transplanted mice (Figure 5E, F). These data suggested increased intestinal absorptive capacity following cold exposure, which is transferable by the microbiota transplantation. We therefore looked at the intestine in more detail, and observed a marked increase in the lengths and weights of the small intestine in the cold exposed mice as early as 9 days after initiation of cold exposure (Figure S5A–C), persisting up to 30 days of cold (Figure 5G, S5D). Microbiota depletion also led to increased intestinal length and weight, however, the changes in this case were more pronounced after 30 days of Abx treatment, and were consistent with the increased intestinal length in the GF mice (Figure 5G–I, S5D). Cold exposure of the Abx and GF mice led to dramatic increases of their intestinal lengths amounting to almost 35%, and weights of over 150% compared to the RT controls, demonstrating remarkable plasticity of the small intestinal absorptive tissue in

response to the increased energy demand (Figure 5G–I, S5D, E). The rest of the tissues, such as the colon, stomach, iBAT, or quadriceps muscle did not show obvious morphological changes (Figure S5D–G), except the decreased WAT levels described above. The increased intestinal length was still present 3 weeks after the end of the cold exposure in the donor mice that were used to transplant the GF mice (Figure 5J, H). Strikingly, cold microbiota transplanted mice also showed a marked increase in the intestinal lengths and weights compared to the RT transplanted controls, suggesting that the microbiota contributed to this phenotype (Figure 5L, M, S5K). To further investigate the changes in the intestinal morphology, we measured the intestinal perimeter and villus length, and found that both were increased in the cold mice, and were further enlarged in the cold exposed Abx mice (Figure 5N–P). This characteristic however was not transferred by the microbiota transplantation, consistent with the proportional increase in the intestinal lengths and weights in the transplanted mice, compared to the donors in which the ratio weight vs. length increased by 1.8 fold.

To investigate the intestinal morphological changes, we quantified the relative contribution of the different cell types composing it - stem cells and Paneth cells in the bottom of the crypt and enterocytes, goblet cells and enteroendocrine cells along the villi. In our models, the number of the enteroendocrine cells was increased in the cold exposed, and cold exposed Abx treated mice, but also in the cold transplanted mice, proportional to the overall increase in the average cell number (Figure S6A–E). There was an antibiotics-dependent effect in the number of goblet cells, which were increased upon microbiota depletion, but no changes were observed in the cold transplanted mice (Figure S6F–H, L,

M). Olfm4 is a highly specific and robust marker for Lgr5 positive stem cells. Quantification of the Olfm4+ cells showed increment only in the intestine of cold exposed Abx treated mice, consistent with their most pronouncedly enlarged intestine (Figure S6I–K). These data suggest that cold exposure leads to a number of changes in the intestinal composition, which in the case of the enteroendocrine cells are in part transferable by cold microbiota transplantation.

Microvilli form the brush border on the apical epithelial surface of the small intestine, and a single enterocyte can have as many as 1000 microvilli, each one formed by cross-linked actin bundles. They increase the surface area of the absorptive cell approximately 25-fold. Using quantitative electron microscopy (EM), we found that the microvilli length is substantially increased in the cold exposed, as well as in microbiota depleted mice (Figure 6A–C), thus further largely increasing the intestinal surface area. Strikingly, these differences were also transferred in the cold microbiota transplanted mice, which showed increased microvilli lengths (Figure 6D–F). Together, these results demonstrate that during increased energy demand, specifically cold exposure, there is a dramatic increase in the intestinal absorptive surface area due to the increased intestinal, villi and microvilli lengths, and that cold microbiota transfer alone can be sufficient to induce these changes.

Reduced apoptosis underlines the increased intestinal surface. To uncover the mechanisms of the microbiota-epithelium crosstalk responsible for the observed gut phenotype, we deep sequenced the transcriptome from proximal jejunum of RT,

RT+Abx, Cold and Cold+Abx mice. The expression profiles markedly differed between the groups (Figure 6G), and unbiased pathway enrichment analysis revealed changes in pathways involved in cytoskeletal remodeling, tissue growth, Wnt signaling, apoptosis and immune response common for mice with increased intestinal surface (Cold, RT+Abx and Cold+Abx), when compared to RT mice (Figure 6H, I, S6N). Anti-microbial response and TNF signaling, which promote apoptosis and cell shedding, and are activated by bacteria through NF-κB and TLR pathways (Hausmann, 2010; Spehlmann and Eckmann, 2009), were strongly suppressed in all microbiota depleted mice (Figure S6N). Indeed, apoptosis and anti-apoptotic interleukin-15 signaling (Obermeier et al., 2006), were among the top regulated pathways in the mice with increased intestinal surface (Figure 6H, I, S6N). Using the TUNEL assay we observed that compared to the RT mice, the apoptosis was markedly reduced in the villi of all other groups (Figure 6J). This phenotype was transferred in the cold transplanted animals, which retained the anti-apoptotic phenotype of the GF and Abx mice (Figure 6K–O). Conversely, RT transplanted mice acquired increased apoptosis, exhibited reduction of the anti-apoptotic *Il15*, *Bcl2l1* (coding isoform Bcl2-XL) and *Mcl1* expression (Pelletier et al., 2002), and showed increased caspase 3 activation (Figure 6M–O). Concomitantly, the mice with increased intestinal surface had augmented vascularization and tissue remodeling gene expression, and showed marked increase in the main apical (Sglt1, gene *Slc5a1*) and basolateral (Glut2, *Slc2a2*) glucose transporters (Figure 6I, M). Together, these data suggest a mechanistic explanation of the increased intestinal surface area and glucose permeability, which can be transferred by the cold microbiota transplantation.

Cold Microbiota Increases Intestinal Absorption in Akkermansia muciniphila-Sensitive Manner. To finally demonstrate that the increased intestinal surface corresponds to enhanced absorptive capacity of the intestine, we did *ex vivo* experiments in isolated segments from the middle to proximal jejunum of the microbiota transplanted mice. Mucosal to serosal D[1-^{14}C] Glucose (D[^{14}C]G) apparent diffusion coefficient was higher in cold transplanted mice (Figure 7A), suggesting increased intestinal glucose absorption. This was consistent with the increased D[^{14}C]G present in intestinal tissue after one hour of transport, and lower residual D[^{14}C]G levels in the lumen (Figure 7B, C). Cold microbiota mice also had prolonged intestinal transit time, proportional to the increase in the intestinal length of the corresponding animals (Figure 7D). Since the increased intestinal surface area was also present in the microbiota depleted mice, we assumed that absence of certain bacterial strains, rather than increased abundance could be responsible for the observed intestinal phenotype following the cold microbiota transplantation. *Akkermansia muciniphila* (*A. muciniphila*) is a Gram-negative bacterium that commonly constitutes 3–5% of the gut microbial community. *A. muciniphila* within the mucus layer is implicated in the control of host mucus turnover (Belzer and de Vos, 2012), which improves gut barrier function, and is linked to obesity (Everard et al., 2013). Since *A. muciniphila* is the most abundant species of the Verrucomicrobia, the most negatively affected phylum in response to cold exposure, we investigated whether this strain alone could revert part of the transplanted phenotype. Co-transplantation of *A. muciniphila* fully prevented the cold microbiota transferable increase of the intestinal glucose absorption (Figure 7A–C), and decreased the intestinal transit time (Figure 7D). Moreover, the increased intestinal length caused by cold microbiota transplantation was

fully reverted in the cold microbiota + *A. muciniphila* transplanted animals (Figure 7E, S7A). These results were consistent with the OGTT, which showed a limited increase in the glucose peak 15 min after the gavage (Figure 7F), and no differences in the insulin levels between the groups (Figure S7B). Neither differences were observed in the tolerance to insulin and cold, nor in the expression of the beige fat markers (Figure S7C–J), together suggesting that *A. muciniphila* does not negatively affect the browning or the sensitivity to insulin. Interestingly, *A. muciniphila* colonization reverted the changes in the Bacteroidetes/Firmicutes ratio in the cold transplanted mice (Figure S7K, L). Therefore, we investigated the importance of the rest of the bacterial consortium by mono-colonizing GF mice with *A. muciniphila* and observed no differences in the intestinal length and duodenum perimeter, while there was a small decrease of the microvilli length bordering significance (Figure S7M–P), suggesting that *A. muciniphila* is necessary, but not sufficient to revert the intestinal lengthening. In contrast, daily gavage of *A. muciniphila* to cold exposed mice decreased their BW and fat mass gain, and shortened their intestine and microvilli already after 7 days of cold exposure. The Bacteroidetes/Firmicutes abundance was not yet affected by the cold exposure at this time interval, showing that changes in their ratio is not a prerequisite for the intestinal remodeling, and that change in *A. muciniphila* precedes the remodeling of these major phyla (Figure 7G–J, S7Q–T). *A. muciniphila* re-colonization during the cold exposure decreased the OGTT peak, and prevented the cold induced increase in the intestinal absorptive capacity (Figure 7K–M, S7U). Accordingly, re-colonizing *A. muciniphila* reverted the cold induced decrease in the apoptosis levels, and reduced the expression of the key tissue remodeling, anti-apoptotic and glucose uptake genes during cold (Figure

7N–Q). Combined, these results underscore that the cold exposure-induced decrease of *A. muciniphila* enables increasing the intestinal absorptive surface by altering several key regulatory pathways, and that co-transfer of this strain together with the cold microbiota, or during the cold exposure is sufficient to prevent the adaptive increase in the intestinal absorptive functions which maximize the caloric uptake during cold.

Discussion

During evolution, mammals developed a number of adaptive responses to energy scarcity. Microbial diversity of the human gut is the result of co-evolution between microbial communities and their hosts. We assumed that this co-evolution favoured maximising uptake of calories from the consumed food during periods of increased energy demand, such as cold exposure. Indeed, cold exposure led to dramatic changes of the microbiota composition, increasing Firmicutes vs. Bacteroidetes ratios, and almost completely depleting the Verrucomicrobia phylum. We found that these changes favoured enhanced energy extraction during cold. Interestingly, in part this is rendered possible by an adaptive mechanism of the host that increases the overall intestinal absorptive surface, due to a marked elongation of the total intestinal, villi and microvilli lengths. When transplanted to GF recipient mice, the cold microbiota alone was sufficient to promote this increased intestinal absorptive surface area by lengthening the gut and the epithelial microvilli. Similar changes in the gut morphology were observed in microbiota depleted mice, which is also a condition of negative energy balance, suggesting that the increase in the intestinal absorptive surface is a general adaptive mechanism promoting caloric uptake when food is available.

In absence of microbiota, epithelial survival was promoted by removal of pro-apoptosis signals, up-regulation of growth factor cascades and increase in glucose transport. Colonization by different gut consortia interfered with these changes to different extents, either keeping most of them (cold microbiota) or restoring them to normal levels (RT or cold+*A.muciniphila* colonization). Cold exposure of the microbiota depleted mice however, further increased the intestinal length, suggesting that additional factors also contribute to this process. The observed increased intestinal absorptive capacity in absence of *A. muciniphila* could give additional explanation to its function in obesity, where absence of this bacterium enables increased uptake in surrounding of excess energy despite the constant intestinal length. This is consistent with our *ex vivo* data that show decreased glucose permeability in presence of *A. muciniphila* in isolated equal (2cm long) jejunal segments, and suggests that absence of this bacterium is necessary, but may not be sufficient to increase the intestinal length. Here we demonstrate that also in conditions of negative energy balance and lean and healthy phenotype, *A. muciniphila* absence enables increased caloric uptake. All this suggest that this bacterium may act as an energy sensor that is abundant during caloric deficiency, and is low when the energy is in excess, as a co-evolutionary mechanism enabling the energy uptake when available. Indeed, *A.muciniphila* is elevated in undernourished mice (Preidis et al., 2015), and in caloric restricted humans (Dao et al., 2015), both typical examples of energy scarcity; while it is absent during cold where food intake is strongly increased. Maintaining the increased gut length and absorptive surface is energy requiring. To ensure that the intestinal lengthening pays off, this process would need to depend on whether the energy

needed to maintain the increased intestinal surface is justified in promoting overall increase in the energy balance, which is not the case in conditions of low food abundance. Seen in this context, *A. muciniphila* is a unique example of host microbial mutualism regulating the energy homeostasis and enabling positive energy balance.

In addition, our data demonstrate that the cold microbiota alone is sufficient to induce tolerance to cold, increased EE as well as lower fat content, and that this effect is at least in part mediated by browning of the white fat depots. This provides mechanistic explanation for the increased insulin sensitivity following cold microbiota transplantation, since increased browning protects against obesity and insulin resistance (Ghorbani et al., 1997; Guerra et al., 1998; Kopecky et al., 1995). *A. muciniphila* on the other hand could not explain the browning following microbiota transplantation, suggesting that additional changes in the intestinal microbiota are mediating this. Thus, discriminating and narrowing down the exact bacterial species affecting this would be an interesting area of future study. Fecal microbiota transplantation was reported almost 50 years ago (Eiseman et al., 1958), and has re-gained interest as a treatment option for several pathologies (Ley et al., 2006) (Kelly, 2013) (Khoruts, 2014). In the context of the increased obesity prevalence and energy unbalance, our study showing microbiota changes that promote weight loss and energy dissipation, imply microbiota as a key player mediating the tight control of the energy homeostasis with large therapeutic potential.

Figure Legends

Figure 1. Cold Exposure Changes the Gut Microbiota Composition

(A) Rectal body temperature (BT) of food restricted, or ad libitum fed C57Bl6J mice after 4 and 8 hours (hr) of cold exposure (n=8 per group).

(B) Change in BT compared to initial as in (A).

(C) Rectal BT after 3 hr of cold exposure of male mice treated or not with antibiotics (n=8 per group).

(D) Rectal BT after 4 hr and 24 hr of cold exposure, in antibiotics treated, or control female mice (n=6 per group).

(E) Change in BT compared to initial as in D.

(F) Principal coordinates analysis (PCoA) based on Weighted UniFrac analysis of OTUs. Each symbol represents a single sample of feces after 31 days of cold exposed (n=8) or RT controls (n=6 per group).

(G) Hierarchical clustering diagram using the average-neighbor (HC-AN) method comparing feces of 31 days cold exposed mice (n=8) and their RT controls (n=6). Associated heat map shows the relative abundance of representative OTUs selected for $p < 0.05$, obtained with a Welch t-test comparison of the two groups, and then grouped into families. One representative OTU with the greatest difference between the two group means from each family is selected for inclusion in the heat map diagram. OTUs is shown as: Phylum, Class, Order, Family, Genus, and Species. R: RT; C: Cold exposed.

(H) Comparison of phylum-level proportional abundance of cecum and feces of up to 31 days cold exposed or RT control mice

(I, J) Richness represented as the proportions of OTUs classified at the phylum rank. in (I) feces, or (J) cecum. In (H), (I) and (J) n=5+6 (cecum), or 6+8 (feces).

(K) Heatmap tree comparing selected OTUs abundance from feces of RT controls (n=6, inner rings) and 31 days cold exposed mice (n=8, outer rings) and their phylogenic relationships. The OTUs representative of differentially abundant families are selected as described in panel H.

See also Figure S1, S2, S3.

Figure 2. Cold Microbiota Transplantation Increases Insulin Sensitivity and WAT Glucose Uptake

(A, B) Intraperitoneal insulin tolerance test (ITT) in RT and 25 days cold-exposed mice (A), or RT and cold microbiota transplanted mice (B) relative to initial blood glucose, (n=8 per group).

(C-E) Euglycemic-hyperinsulinemic clamp of awake mice as in (A). Rate of disappearance of ^{3}H-D-glucose (C). GIR time course during the hyperinsulinemic clamp (D). 2[^{14}C]DG uptake in various tissues (E) (n=6+6).

(F) 2[^{14}C]DG tracer uptake in tissues 45min after IP tracer and glucose (2g/kg BW) administration in mice as in (A) (n=6 per group).

(G, H) 2[^{14}C]DG uptake in tissues 30 min after administration under basal conditions in anesthetized RT (n=9) and cold (n=10) (G); or RT and cold transplanted mice (n=3) (H).

(I, J, L) Positron emission tomography-computer tomography (microPET-CT) measurement of [^{18}F]FDG uptake in ingSAT (I), pgVAT (J), or quadriceps muscle (L) in basal conditions of RT and cold transplanted mice as in (B). (n=6 per group).

(K) Transversal [^{18}F]FDG PET-CT images of ingSAT and pgVAT of mice as in (I, J). See also Figure S4.

Figure 3. Cold Microbiota Promotes Browning of WAT

(A) 3D reconstitution of the ingSAT and pgVAT of cold and RT transplanted mice 21 days after transplantation using the CT scans. Bar: 5mm.

(B) Weight of fat pads of cold or RT transplanted mice after 5.5 weeks (n=6 per group).

(C–H) IngSAT, or pgVAT volumes (C, E); or densities (G, H) of mice as in (A). Change in each fat pad volume (D, F) (n=12 per group, except (E, F) where n=6 per group) of same mice scanned at day 3, and day 21 after transplantation.

(I, J) Cell size profiling of adipocytes from ingSAT (I), or pgVAT (J) of RT or cold transplanted mice 21 days after transplantation. The values show % from the total number of analyzed cells. Bars show mean of the pooled corresponding fractions from each animal ± sem (n=6 for each panel).

(K, L) H&E staining on paraffin sections from ingSAT (K), or pgVAT (L) of RT or cold transplanted mice.

(M, O, P) Relative mRNA expression in ingSAT (M), pgVAT (O), or iBAT (P) of RT or cold transplanted mice (n=6 per group), quantified by real-time PCR and normalized to the house keeping beta-2-microglobulin (B2M).

(N) Immunohistochemistry of Ucp1 and DAPI on paraffin sections from ingSAT in RT or cold transplanted mice as in (K).

(Q) Resting energy expenditure (REE) in RT or cold transplanted mice, measured between day 3 and day 21 after bacterial colonization (n=6 per group).

Scale in (K), (L) and (N): 100μm.

Figure 4. Cold Microbiota Prevents Hypothermia

(A, B) Rectal temperature (A), or temperature change (B), of RT or cold transplanted mice before, or after 4 hr of cold exposure (n=8 per group).

(C) Infrared images of representative RT or cold transplanted mice after 4 hr cold exposure.

(D–F) Infrared temperature readings from eye (D), ventral (E), or dorsal (F) region of mice as in (C) before, or after 4 hr cold exposure.

(G–I) Infrared temperature readings from eye (G), ventral (H), or dorsal (I) region of mice as in (C) before, or after 12 hr cold exposure.

Figure 5: Cold Exposed, and Cold Microbiota Transplanted Mice Show Increased Intestinal Length and Caloric Uptake

(A, B). Oral glucose tolerance test (OGTT) of cold exposed mice with or without Abx treatment (A); or RT and cold microbiota transplanted mice 16 days after transplantation (B) (n=8 per group).

(C, D) Plasma triglycerides (C) and free fatty acids (D) during oral fat tolerance test in RT or cold microbiota transplanted mice as in (B) (n=6 per group).

(E, F) Total caloric uptake during 24hrs of cold or RT exposed (E), or transplanted (F) mice (n=8 per group). Mice were kept 2 per cage. Each cage was considered as one pooled sample (n=4). Data in E and F show mean±sem.

(G, H) Small intestine and colon lengths of cold exposed mice with or without Abx treatment (n=8 per group) (G); or cold exposed and RT kept GF mice(n=6 per group) (H).

(I) Representative images of cecum, small and large intestine of mice as in (E–H).

(J) Small intestine and colon lengths of 30 days cold exposed or RT kept donor mice used for microbiota-transplantation, 23 days after start of cohabitation at RT(n=6 per group).

(K) Stomach, small intestine, cecum and colon weights of donor mice as in (J).

(L) Small intestine and colon lengths of RT or cold microbiota transplanted mice as in (B) (n=8 per group), 21 days after transplantation, and GF controls (n=4).

(M) Representative images of cecum, small and large intestine of mice as in (L).

(N–P) H&E staining of duodenum of cold exposed mice with or without Abx treatment (N), and morphometric quantifications of duodenal perimeter (O) and villi length (P) (n=8 per group in triplicates, data show mean±sem).

See also Figure S5 and S6.

Figure 6: Presence and Composition of Microbiota Determines Length of Microvilli on Brush Border of Small Intestine

(A, D) Electron micrographs of jejunal enterocyte microvilli of cold exposed mice with or without Abx treatment (A); or GF, RT and cold microbiota transplanted mice 19 days after transplantation (D). Scale: 2µm.

(B, E) Morphometric quantification of microvilli length distribution in (B) as in (A); and (E) as in (D).

(C, F) Average microvilli lengths of mice as in (A, and D respectively).

(G) Principal component analysis (PCoA) of gene expression data in proximal jejunum of mice as in (A).

(H) Top commonly regulated pathways (MetaCore pathway enrichment) in RT, RT+Abx, Cold and Cold+Abx differential gene expression comparisons. Legend: 1. Immune response: TNF-R2 signaling; 2. Main growth factor signaling cascades; 3. IGF family signaling in colorectal cancer; 4. c-Kit ligand signaling during hemopoiesis; 5. Apoptosis and survival; 6. GM-CSF signaling; 7. TGF, WNT and cytoskeletal remodelling; 8. Signal transduction: AKT signalling; 9. Cell adhesion: Chemokines and adhesion; 10. IL-15 signaling via JAK-STAT cascade.

(I, M) Relative mRNA expression in proximal jejunum of mice as in (A); or GF, or RT and cold microbiota transplanted GF (M), quantified by real-time PCR and normalized to the average expression of the house keeping *Rplp0* (36b4) and *Rsp16* (GF are n=4; rest are n=8 per group).

(J, K) Terminal deoxynucleotidyl transferase (dUTP) nick end labeling (TUNEL) assay for apoptotic cells double labeled with DAPI of proximal jejunum paraffin sections of mice as in (A), or in (D). Scale: 200μm.

(L) Semi-fine 1μm tick EM sections of proximal jejunum stained with toluidine blue displaying apoptotic cells in dark blue (marked with arrowheads) of mice as in (D). Round are Goblet cells. Scale: 20μm.

(N, O) Western blotting of lysates from proximal jejunum of mice as in (D) and (A), and respective quantifications (O) normalized to loading controls.

See also Figure S6.

Figure 7. Cold Microbiota Increases Intestinal Absorption Due to Absence of *A. muciniphila*

(A–C) *Ex-vivo* measurements of glucose transport in jejunal segments excised from RT, cold and cold+*A.muciniphila* transplanted mice (n=5 per group) - with mucosal to serosal glucose permeability (A); radioactive glucose tracer in tissue (B); and in the lumen (C), of jejunum segment after 1h of transport.

(D) Intestinal transit time of RT, cold and cold + *A. muciniphila* transplanted mice as in (A) (n=6 per group).

(E) Intestinal length in mice transplanted with RT (n=9), cold (n=10) and cold+ *A.muciniphila* (n=6) microbiota 6 weeks after transplantation.

(F) OGTT in cold (n=10) and cold + *A .muciniphila* (n=6) transplanted male mice as in (A).

(G) Body weight change compared to day 0 of 7 weeks old mice, exposed to cold for 7 days and gavaged daily with fresh *A.muciniphila* or vehicle (PBS) (n=5 per group).

(H) Intestinal length of mice as in (G).

(I) Electron micrographs of jejunal enterocyte microvilli of mice as in (G) Scale: 2µm.

(J) Morphometric quantification of microvilli length distribution of the EM images as shown in (I) (n=5 per group).

(K) OGTT of mice as in (G) 6 days after start of treatment.

(L, M) *Ex-vivo* measurements of glucose transport in jejunal segments excised from mice as in (G) (n=5 per group) - with mucosal to serosal glucose permeability (L); radioactive glucose tracer in tissue after 1h of transport (M).

(N) TUNEL assay for apoptotic cells double labeled with DAPI of proximal jejunum paraffin sections of mice as in (G). Bar: 200µm.

(O) Semi-fine 1µm tick EM sections of proximal jejunum stained with toluidine blue showing apoptotic cells in dark blue (marked with arrowheads). Round are Goblet cells. Bar: 20µm.

(P, Q) Relative mRNA expression in proximal jejunum of mice as in (G) or (A) ((P), or (Q) respectively), quantified by real-time PCR and normalized to the average expression of the house keeping *Rplp0* (36b4) and *Rsp16*.

See also Figure S7.

Experimental Procedures

Animals. All C57Bl/6J (wild-type (wt)) mice (Charles River, France) were kept in a specific pathogen free facility (SPF) in 12 hr day/night cycles, unless otherwise specified. Germ-free (GF) mice were on C57Bl/6 background from the germ-free facility of the University of Bern, and were kept in sterile conditions until sacrifice, unless otherwise stated. All mice were kept 2 per cage. Fresh antibiotics were administered in the drinking water and changed once a week as described (Grivennikov et al., 2012), containing 100µg/ml Neomycin, 50µg/ml Streptomycin, 100U/ml Penicillin, 50µg/ml Vancomycine, 100µg/ml Metronidazole, 1mg/ml Bacitracin, 125µg/ml Ciprofloxacin, 100µg/ml Ceftazidime and 170µg/ml Gentamycin (Sigma, Germany; Alkaloid, Macedonia). Cold exposures were done at 6°C in a light and humidity controlled climatic chamber (TSE, Germany) in SPF conditions using individually ventilated cages. Acclimatized animals were allocated to groups based on their body weights and blood glucose levels to ensure

equal starting points. Microbiota transplantations were done by co-housing GF mice with cold exposed donors at RT for 10 days. Mice were treated with *A. muciniphila* by oral gavage at a dose $2x10^8$ cells/0.2ml suspended in sterile anaerobic PBS as previously described (Everard et al., 2013). All experiments were started in 7-8 weeks old mice and male unless otherwise specified. All animal experiments were approved by the Swiss federal and Geneva cantonal authorities for animal experimentation.

Statistical Analysis. Unless otherwise specified in the figure legends, significance was calculated using non-paired two-tailed Student's t-test.*: $p \leq 0.05$, **: $p \leq 0.01$, ***: $p \leq 0.001$, Brackets [ ] show comparisons of all pairs in the dataset. All values show mean ± sd. All experiments were done at least three times, and the representative experiment is shown. Sample sizes and animal numbers were chosen based on power calculations of 0.8.

Accession Numbers. NCBI GEO accession number for all the sequencing data is GSE74228.

Supplemental Information. Includes Supplemental Experimental Procedures, seven figures and three tables.

Author Contributions

C.C., O.S., N.S.Z., V.T., D.R., S.F. and A.S designed and performed experiments and analyzed data. D.J.C., Y.S. and X.M. did PET-CT and CT measurements, N.Z. measured

metabolites, S.H. and S.H. provided GF mice and participated in mono-colonizations. M.T. designed the work, performed experiments, analyzed data, prepared the figures and wrote the manuscript with input from all co-authors.

Acknowledgments

We thank Maria Gustafsson Trajkovska, Claes Wollheim and Roberto Coppari for discussions and critical reading; Jean-Baptiste Cavin and André Bado for sharing expertise in intestinal loop; Christian Darimont for help with bomb calorimetry; Abdessalam Cherkaoui and Jacques Schrenzel for the use of anaerobic incubator; [ERC-2013-StG-281904] to SH for partial support of the gnotobiotic research; Mirosava Ilievska for providing antibiotics; and Mario Kreutzfeldt and Prof Doron Merkler for help with histology quantifications.

The research leading to these results has received funding from the European Research Council under the European Union's Seventh Framework Programme (FP/2007-2013) / ERC Grant Agreement n. 336607 [ERC-2013-StG-336607]; the Louis-Jeantet Foundation; Fondation pour Recherches Médicales; Novartis Foundation (14B053); and the Swiss National Science Foundation (SNSF) Professorship (PP00P3_144886) to MT.

References

Backhed, F., Ding, H., Wang, T., Hooper, L.V., Koh, G.Y., Nagy, A., Semenkovich, C.F., and Gordon, J.I. (2004). The gut microbiota as an environmental factor that regulates fat storage. Proceedings of the National Academy of Sciences of the United States of America *101*, 15718-15723.

Badman, M.K., and Flier, J.S. (2005). The gut and energy balance: visceral allies in the obesity wars. Science *307*, 1909-1914.

Belzer, C., and de Vos, W.M. (2012). Microbes inside--from diversity to function: the case of Akkermansia. The ISME journal *6*, 1449-1458.

Cannon, B., and Nedergaard, J. (2004). Brown adipose tissue: function and physiological significance. Physiol Rev *84*, 277-359.
Chou, C.J., Membrez, M., and Blancher, F. (2008). Gut decontamination with norfloxacin and ampicillin enhances insulin sensitivity in mice. Nestle Nutr Workshop Ser Pediatr Program *62*, 127-137; discussion 137-140.
Cousin, B., Cinti, S., Morroni, M., Raimbault, S., Ricquier, D., Penicaud, L., and Casteilla, L. (1992). Occurrence of brown adipocytes in rat white adipose tissue: molecular and morphological characterization. J Cell Sci *103 (Pt 4)*, 931-942.
Dao, M.C., Everard, A., Aron-Wisnewsky, J., Sokolovska, N., Prifti, E., Verger, E.O., Kayser, B.D., Levenez, F., Chilloux, J., Hoyles, L.*, et al.* (2015). Akkermansia muciniphila and improved metabolic health during a dietary intervention in obesity: relationship with gut microbiome richness and ecology. Gut.
Eiseman, B., Silen, W., Bascom, G.S., and Kauvar, A.J. (1958). Fecal enema as an adjunct in the treatment of pseudomembranous enterocolitis. Surgery *44*, 854-859.
El Kaoutari, A., Armougom, F., Gordon, J.I., Raoult, D., and Henrissat, B. (2013). The abundance and variety of carbohydrate-active enzymes in the human gut microbiota. Nature reviews Microbiology *11*, 497-504.
Everard, A., Belzer, C., Geurts, L., Ouwerkerk, J.P., Druart, C., Bindels, L.B., Guiot, Y., Derrien, M., Muccioli, G.G., Delzenne, N.M.*, et al.* (2013). Cross-talk between Akkermansia muciniphila and intestinal epithelium controls diet-induced obesity. Proceedings of the National Academy of Sciences of the United States of America *110*, 9066-9071.
Farooqi, I.S., and O'Rahilly, S. (2005). Monogenic obesity in humans. Annual review of medicine *56*, 443-458.
Ferreyra, J.A., Wu, K.J., Hryckowian, A.J., Bouley, D.M., Weimer, B.C., and Sonnenburg, J.L. (2014). Gut microbiota-produced succinate promotes C. difficile infection after antibiotic treatment or motility disturbance. Cell host & microbe *16*, 770-777.
Ghorbani, M., Claus, T.H., and Himms-Hagen, J. (1997). Hypertrophy of brown adipocytes in brown and white adipose tissues and reversal of diet-induced obesity in rats treated with a beta3-adrenoceptor agonist. Biochem Pharmacol *54*, 121-131.
Grivennikov, S.I., Wang, K., Mucida, D., Stewart, C.A., Schnabl, B., Jauch, D., Taniguchi, K., Yu, G.Y., Osterreicher, C.H., Hung, K.E.*, et al.* (2012). Adenoma-linked barrier defects and microbial products drive IL-23/IL-17-mediated tumour growth. Nature *491*, 254-258.
Guerra, C., Koza, R.A., Yamashita, H., Walsh, K., and Kozak, L.P. (1998). Emergence of brown adipocytes in white fat in mice is under genetic control. Effects on body weight and adiposity. J Clin Invest *102*, 412-420.
Guerra, C., Navarro, P., Valverde, A.M., Arribas, M., Bruning, J., Kozak, L.P., Kahn, C.R., and Benito, M. (2001). Brown adipose tissue-specific insulin receptor knockout shows diabetic phenotype without insulin resistance. The Journal of clinical investigation *108*, 1205-1213.
Hausmann, M. (2010). How bacteria-induced apoptosis of intestinal epithelial cells contributes to mucosal inflammation. International journal of inflammation *2010*, 574568.

Kelly, C.P. (2013). Fecal microbiota transplantation--an old therapy comes of age. The New England journal of medicine *368*, 474-475.
Khoruts, A. (2014). Faecal microbiota transplantation in 2013: developing human gut microbiota as a class of therapeutics. Nature reviews Gastroenterology & hepatology *11*, 79-80.
Kopecky, J., Clarke, G., Enerback, S., Spiegelman, B., and Kozak, L.P. (1995). Expression of the mitochondrial uncoupling protein gene from the aP2 gene promoter prevents genetic obesity. J Clin Invest *96*, 2914-2923.
Koren, O., Goodrich, J.K., Cullender, T.C., Spor, A., Laitinen, K., Backhed, H.K., Gonzalez, A., Werner, J.J., Angenent, L.T., Knight, R., *et al.* (2012). Host remodeling of the gut microbiome and metabolic changes during pregnancy. Cell *150*, 470-480.
Ley, R.E., Turnbaugh, P.J., Klein, S., and Gordon, J.I. (2006). Microbial ecology: human gut microbes associated with obesity. Nature *444*, 1022-1023.
Liou, A.P., Paziuk, M., Luevano, J.M., Jr., Machineni, S., Turnbaugh, P.J., and Kaplan, L.M. (2013). Conserved shifts in the gut microbiota due to gastric bypass reduce host weight and adiposity. Science translational medicine *5*, 178ra141.
Lowell, B.B., V, S.S., Hamann, A., Lawitts, J.A., Himms-Hagen, J., Boyer, B.B., Kozak, L.P., and Flier, J.S. (1993). Development of obesity in transgenic mice after genetic ablation of brown adipose tissue. Nature *366*, 740-742.
Murphy, K.G., and Bloom, S.R. (2006). Gut hormones and the regulation of energy homeostasis. Nature *444*, 854-859.
Obermeier, F., Hausmann, M., Kellermeier, S., Kiessling, S., Strauch, U.G., Duitman, E., Bulfone-Paus, S., Herfarth, H., Bock, J., Dunger, N., *et al.* (2006). IL-15 protects intestinal epithelial cells. European journal of immunology *36*, 2691-2699.
Pelletier, M., Ratthe, C., and Girard, D. (2002). Mechanisms involved in interleukin-15-induced suppression of human neutrophil apoptosis: role of the anti-apoptotic Mcl-1 protein and several kinases including Janus kinase-2, p38 mitogen-activated protein kinase and extracellular signal-regulated kinases-1/2. Febs Lett *532*, 164-170.
Preidis, G.A., Ajami, N.J., Wong, M.C., Bessard, B.C., Conner, M.E., and Petrosino, J.F. (2015). Composition and function of the undernourished neonatal mouse intestinal microbiome. The Journal of nutritional biochemistry.
Ridaura, V.K., Faith, J.J., Rey, F.E., Cheng, J., Duncan, A.E., Kau, A.L., Griffin, N.W., Lombard, V., Henrissat, B., Bain, J.R., *et al.* (2013). Gut microbiota from twins discordant for obesity modulate metabolism in mice. Science *341*, 1241214.
Sato, T., Vries, R.G., Snippert, H.J., van de Wetering, M., Barker, N., Stange, D.E., van Es, J.H., Abo, A., Kujala, P., Peters, P.J., *et al.* (2009). Single Lgr5 stem cells build crypt-villus structures in vitro without a mesenchymal niche. Nature *459*, 262-265.
Sekirov, I., Russell, S.L., Antunes, L.C., and Finlay, B.B. (2010). Gut microbiota in health and disease. Physiological reviews *90*, 859-904.
Sommer, F., and Backhed, F. (2013). The gut microbiota--masters of host development and physiology. Nature reviews Microbiology *11*, 227-238.
Spehlmann, M.E., and Eckmann, L. (2009). Nuclear factor-kappa B in Intestinal protection and destruction. Curr Opin Gastroen *25*, 92-99.
Turnbaugh, P.J., Ley, R.E., Mahowald, M.A., Magrini, V., Mardis, E.R., and Gordon, J.I. (2006). An obesity-associated gut microbiome with increased capacity for energy harvest. Nature *444*, 1027-1031.

Wichmann, A., Allahyar, A., Greiner, T.U., Plovier, H., Lunden, G.O., Larsson, T., Drucker, D.J., Delzenne, N.M., Cani, P.D., and Backhed, F. (2013). Microbial modulation of energy availability in the colon regulates intestinal transit. Cell host & microbe *14*, 582-590.
Wu, J., Bostrom, P., Sparks, L.M., Ye, L., Choi, J.H., Giang, A.H., Khandekar, M., Virtanen, K.A., Nuutila, P., Schaart, G., *et al.* (2012). Beige adipocytes are a distinct type of thermogenic fat cell in mouse and human. Cell *150*, 366-376.
Wu, J., Cohen, P., and Spiegelman, B.M. (2013). Adaptive thermogenesis in adipocytes: Is beige the new brown? Genes Dev *27*, 234-250.
Young, P., Arch, J.R., and Ashwell, M. (1984). Brown adipose tissue in the parametrial fat pad of the mouse. FEBS Lett *167*, 10-14.

Figure 1

Click here to download Figure Figure_1.pdf

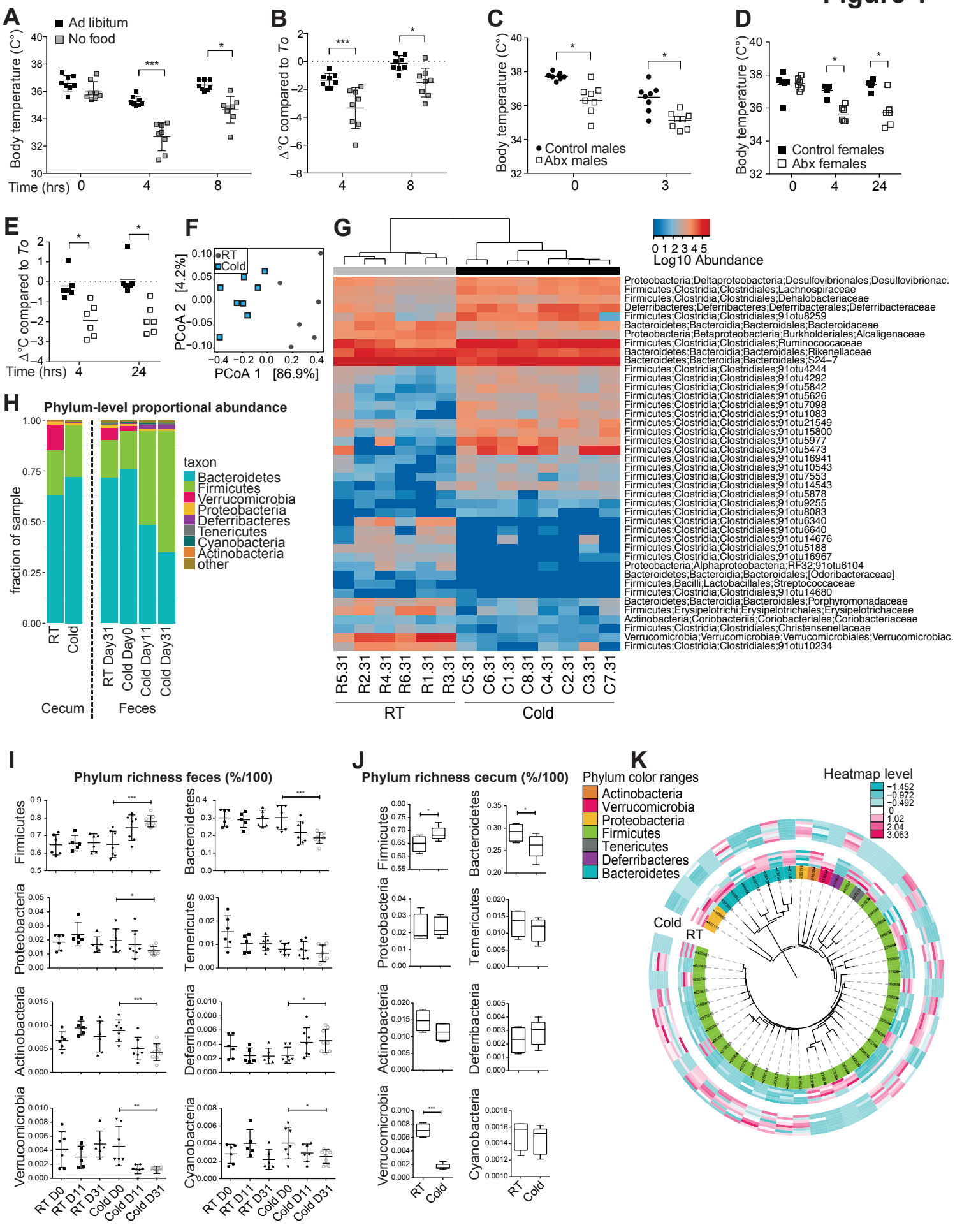

Figure 2

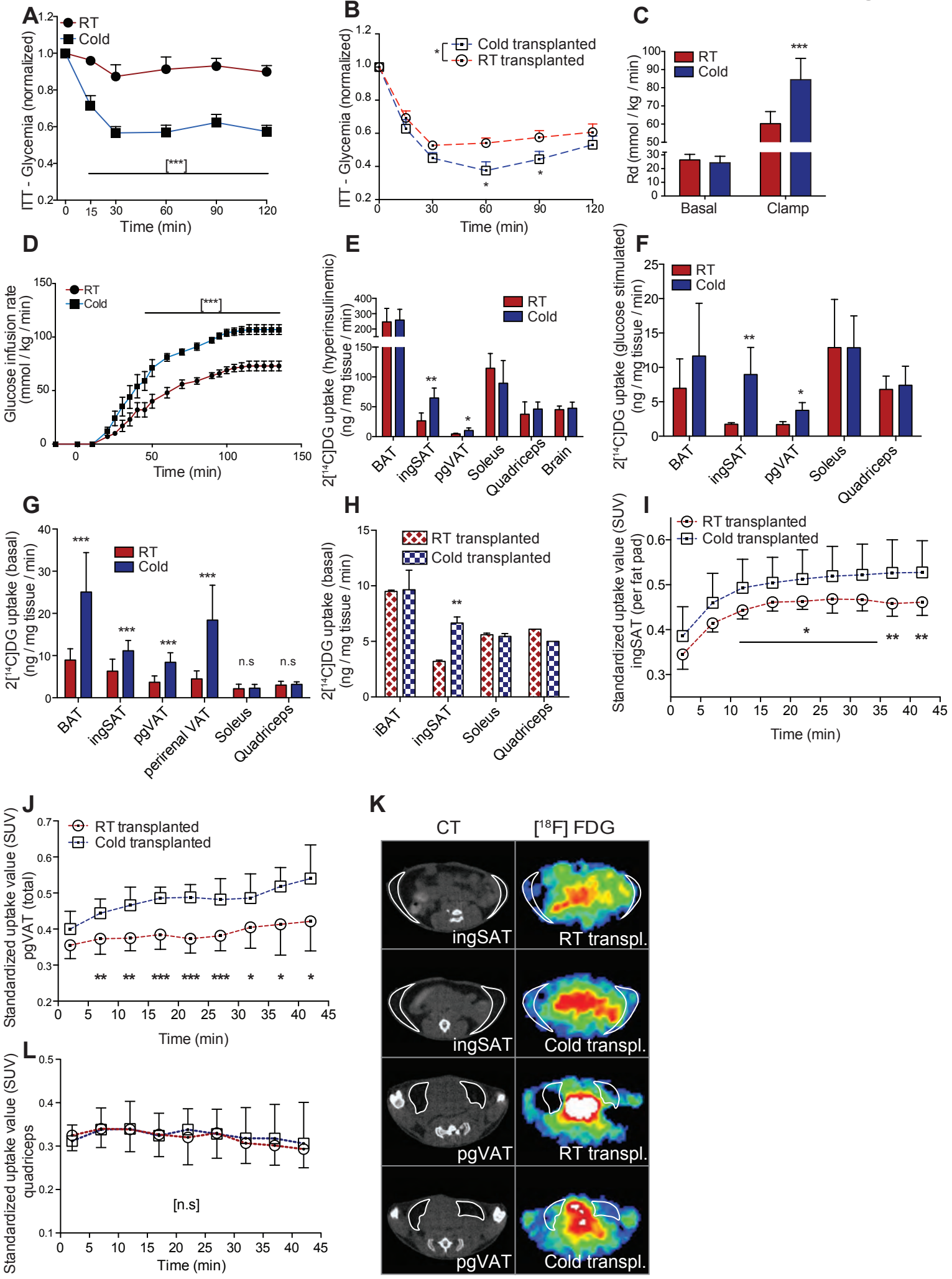

Figure 3

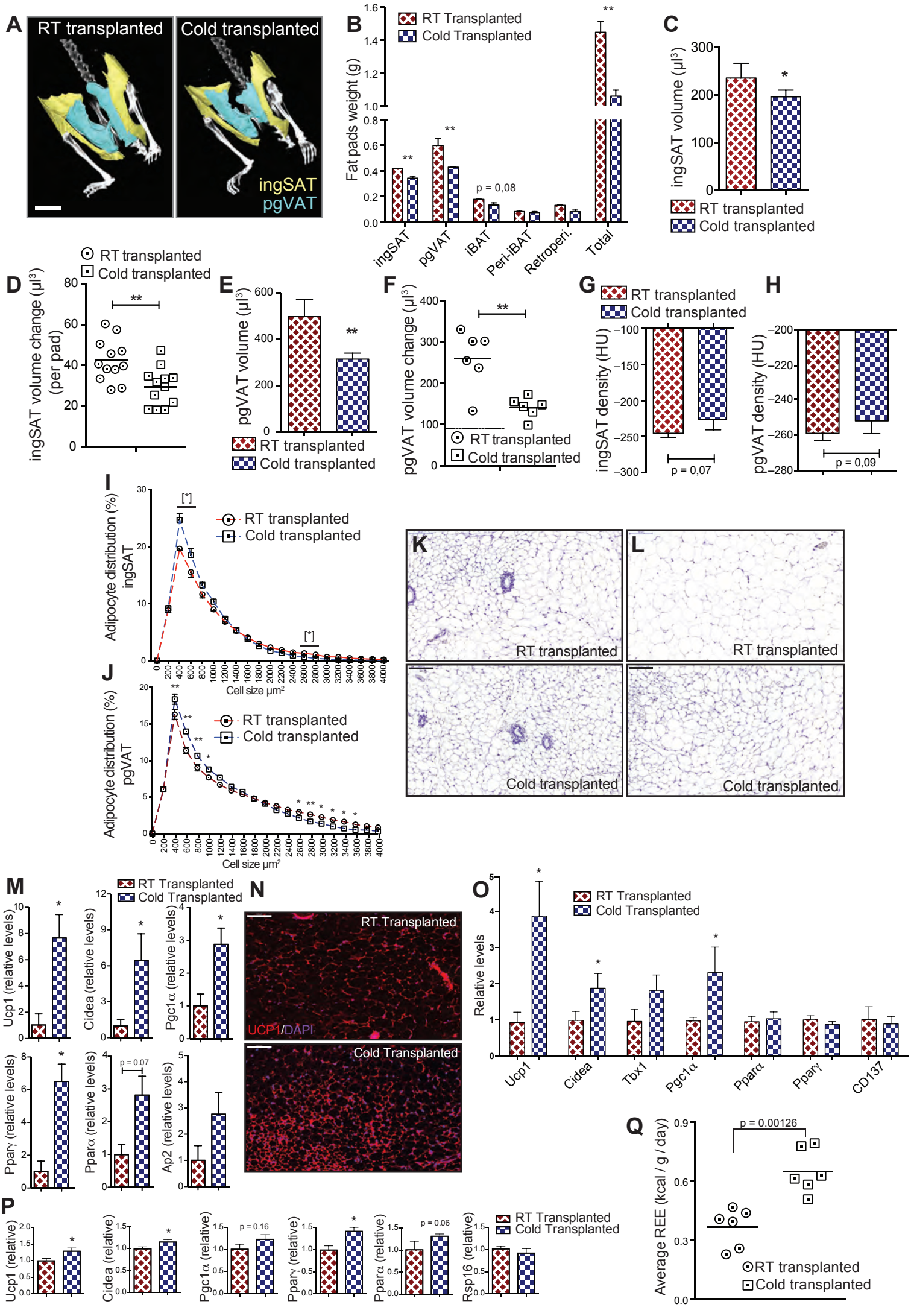

Figure 4

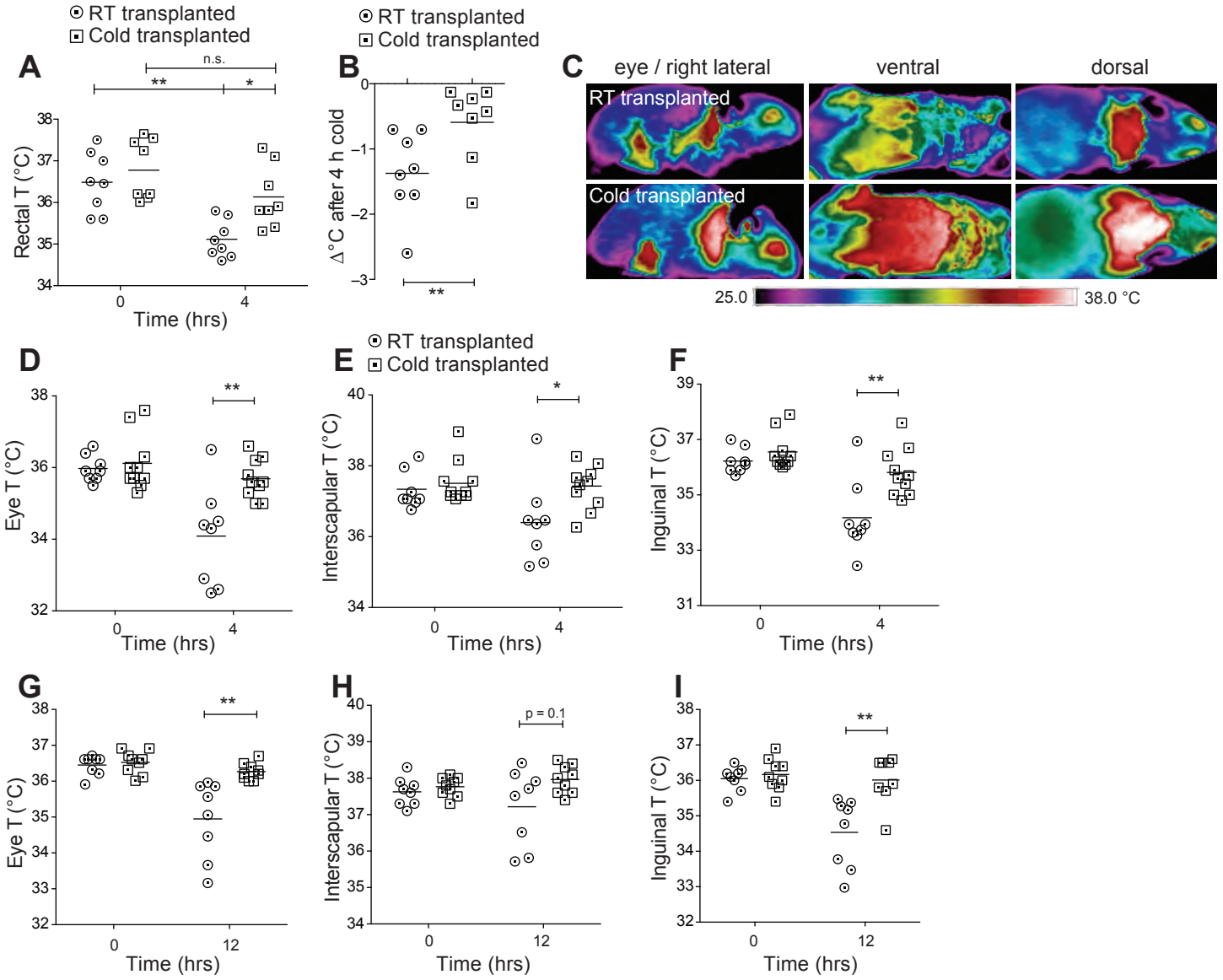

Figure 5

Click here to download Figure Figure_5.pdf

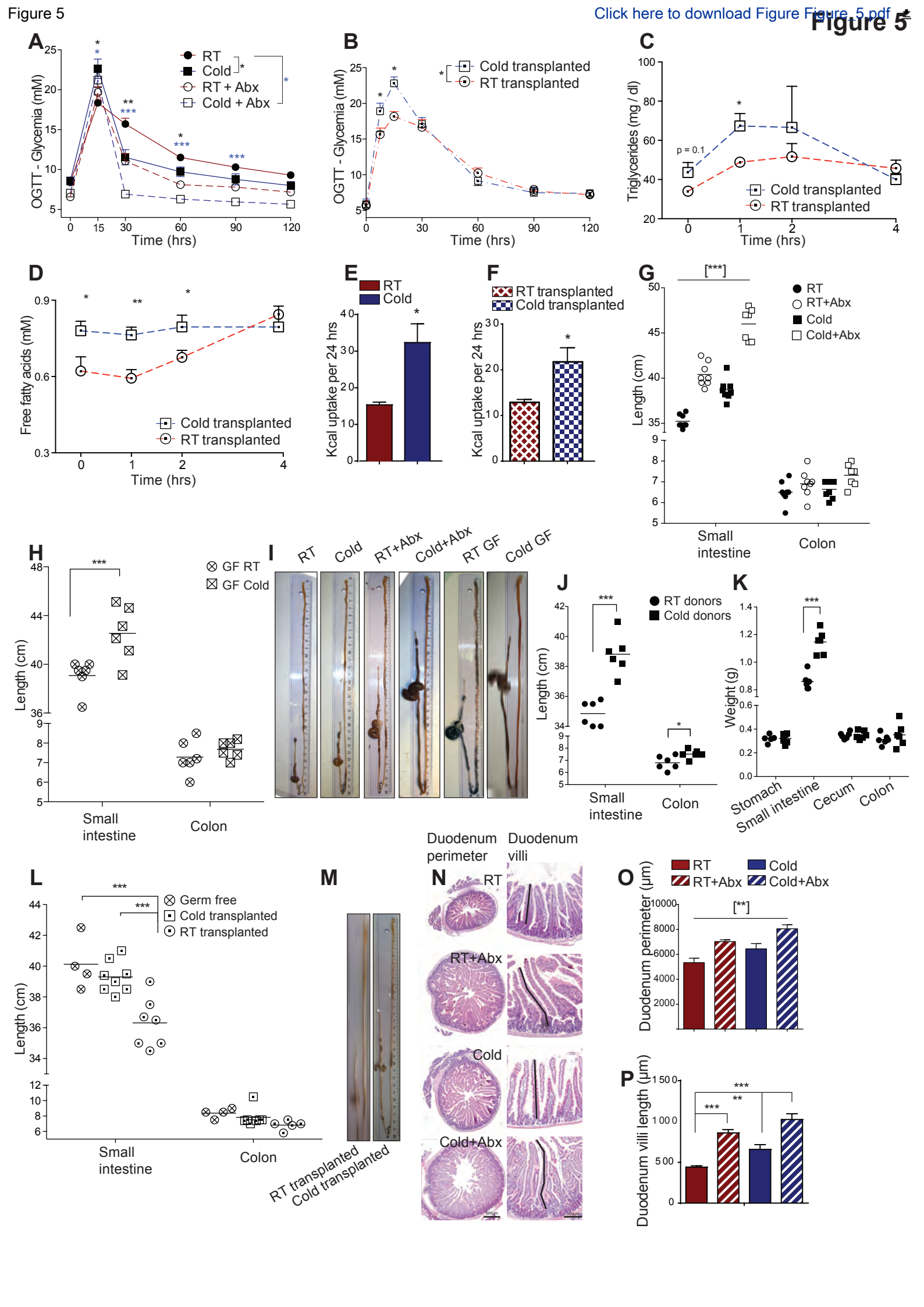

Figure 6

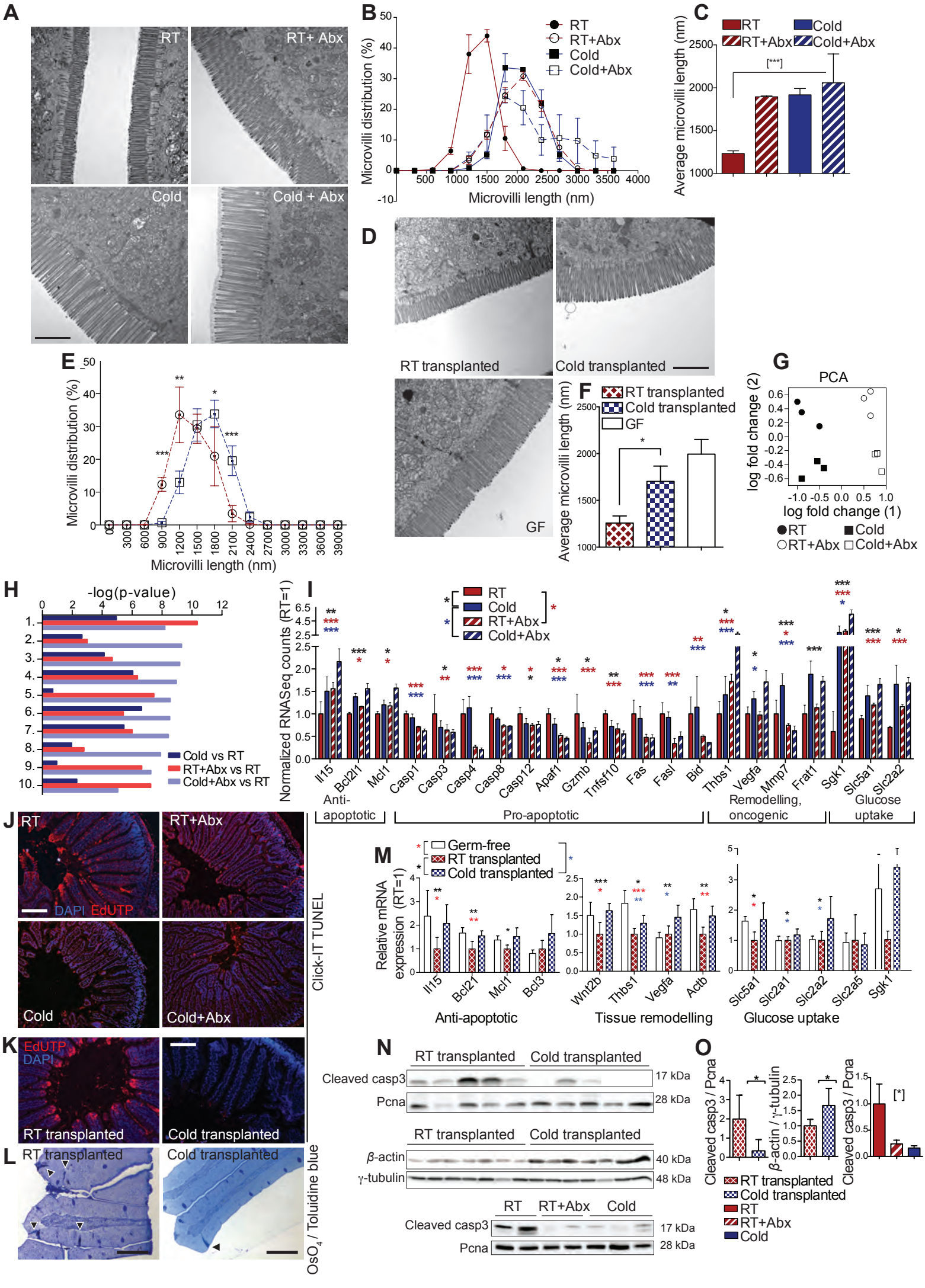

Figure 7

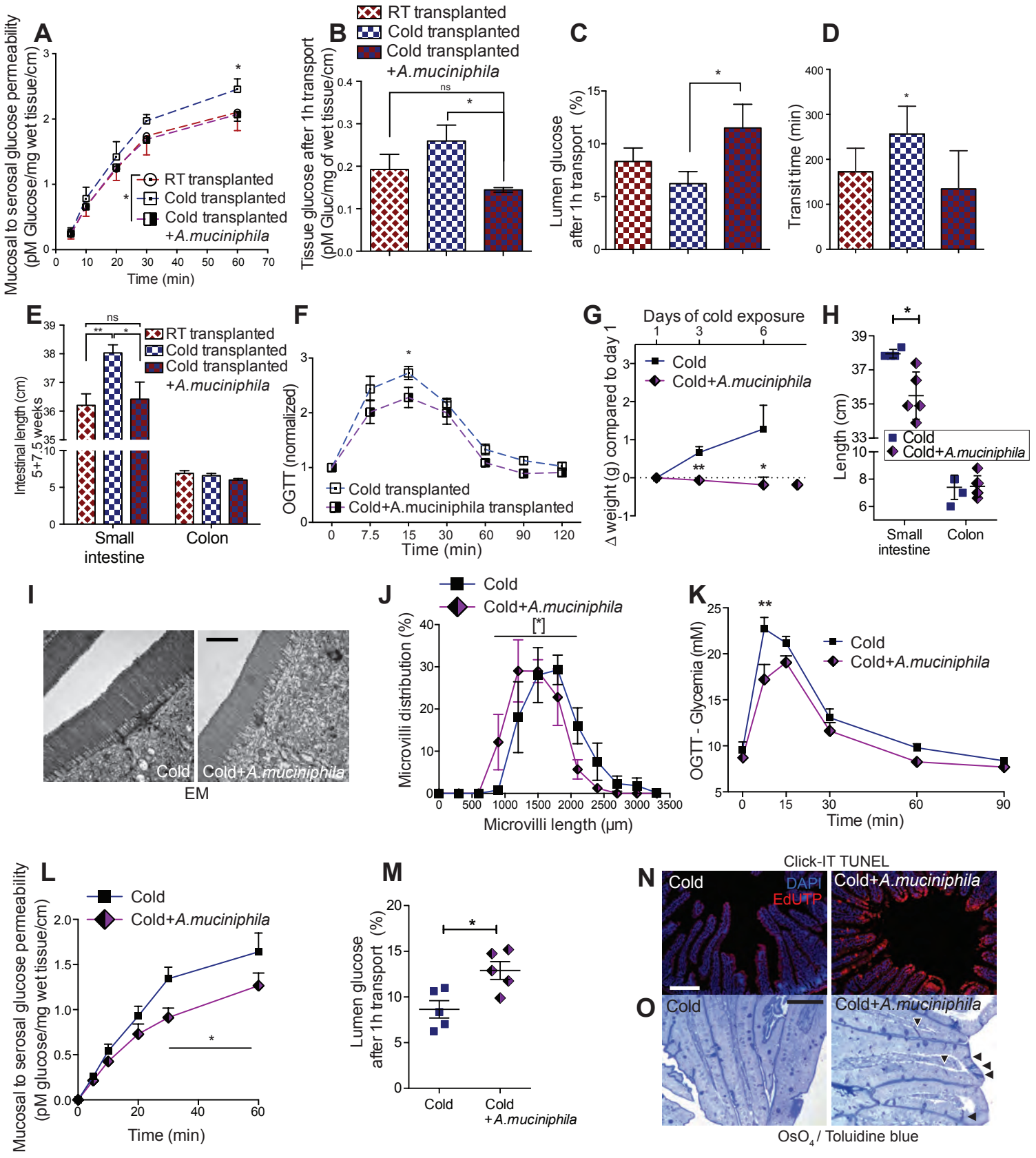

Supplemental Experimental Procedures, Supplemental Tables, and Supplemental References

1) Supplemental Experimental Procedures

Animals. All C57Bl/6J (wild-type (wt)) mice (Charles River, France) were kept in a specific pathogen free facility (SPF) in 12 hr day/night cycles in individually ventilated cages (IVC), unless specified otherwise for the GF or the conventional zone. All mice were kept 2 per cage. All experiments were started on 7-8 weeks old mice. Acclimatized animals were allocated to experimental groups based on their body weights and blood glucose levels to ensure equal starting points. For depletion of microbiota, fresh antibiotics were administered once a week in the drinking water as described previously (Grivennikov et al., 2012), containing 100µg/ml Neomycin, 50µg/ml Streptomycin, 100U/ml Penicillin, 50µg/ml Vancomycine, 100µg/ml Metronidazole, 1mg/ml Bacitracin, 125µg/ml Ciprofloxacin, 100µg/ml Ceftazidime, and 170µg/ml Gentamycin (Sigma, Germany; Alkaloid, Macedonia). Microbiota depletion was confirmed by plating feces on 5% sheep blood agar plates on anaerobic and aerobic conditions; and by qPCR. For the conventional zone, open cages covered with filter lids were used. Cold exposures were performed at 6°C in a light and humidity controlled (40%) climatic chamber (TSE, Germany) for the SPF conditions, or in MEDI1300 from Froilabo for the conventional facility. Germ-free (GF) mice were on C57Bl/6 background maintained germ-free in flexible film axenic isolators at the Genaxen Clean Mouse of the University of Bern, and were kept in sterile conditions until sacrifice, unless otherwise stated. Microbiota transplantations were done by co-housing GF mice with 4 weeks cold exposed or RT donors at room temperature for 10 days. *A. muciniphila* (ATTC BAA-835) was grown anaerobically at 37°C in Schaedler Broth+VitK3 (Biomerieux). Growth and viability of the cells were confirmed by gram staining, qPCR and electron microscopy that showed the same morphology as described previously (Derrien et al., 2008). Freshly grown *A. muciniphila* culture, resuspended in sterile anaerobic PBS was given to mice by oral gavage at a dose of $2x10^8$ cells in 0.2 ml of suspension, as previously described (Everard et al., 2013). For *A. muciniphila* resupply in cold exposed mice, gavage was performed

daily, and for GF mice *A. muciniphila* was monocolonized once. Repopulation was confirmed by qPCR using primers given in Table S3, after bacterial DNA extraction from fresh feces sample collected 24h after gavage (Quiagen Fast-DNA stool kit). All animal experiments were approved by the Swiss federal and Geneva cantonal authorities for animal experimentation.

Gut Microbiota Profiling. Fresh feces and cecum samples were collected, immediately frozen and stored. Bacterial DNA content was extracted using QIAamp Fast DNA stool Mini Kit (Qiagen). Bacterial DNA was PCR amplified with barcoded universal bacterial primers targeting variable regionV4 of 16SrRNA gene. Samples were pooled and sequenced with Ilumina MiSeq platform. Using QIIME and custom scripts, sequences were quality filtered and demultiplexed using exact matches to the supplied DNA barcodes. Resulting sequences were then searched against the Greengenes reference database of 16S rRNA gene sequences, clustered at 97% by uclust. The longest sequence from each Operation Taxonomic Unit (OTU) thus formed was then considered as the OTU representative sequence, and assigned taxonomic classification via Mothur's Bayesian classifier, trained against the Greengenes database clustered at 98%.
The bar chart in Figure 1H, representing phyla abundance displays the 8 phyla with the greatest number of sequences found by summing the number of reads from the OTUs within the phyla; the rest are summed in "other". Each graph in Figure 1I and J, representing phyla richness represents the sum of number of detected OTUs in the phylum relative to the total number of OTUs detected.

Metabolic Experiments. Body temperature was read with infrared camera FLIR E60 (FLIR, UK) from 40cm distance perpendicular to the region of interest (eye, dorsal or ventral region) and the data was analyzed by FLIR Tools+ software. We confirmed the consistency with the results by rectal body temperature measurements. Glucose tolerance test were performed after 12h overnight fasting by intraperitoneal injection or oral gavage of glucose bolus (2g/kg BW). Insulin tolerance test was performed after 6h daytime fast, 0.75U/kg (Sigma Aldrich I9278). All mice were sacrificed after 5h fasting. 500µl of blood was taken from terminally anesthetized mice in tubes with 15ul of 0.5 mM EDTA,

4 µl of aprotinin (1.3%) and 4 µl of DPP-IV (10mM) and plasma stored at -80 °C. Triglycerides were measured by Trig/GB kit (Roche), free fatty by NEFA-HR kit (Wako).

Metabolomic Analysis. Metabolites were extracted from plasma, cecum and feces as previously described (Fiehn and Kind, 2007). Briefly, 400µl for 30µl of plasma and 20x w/vol for feces and cecum of degassed chilled acetone:isopropanol (2:1 ratio) was added, vortexed, shaken 5min at cold, then centrifuged to pellet cell debris and protein. Metabolites were analyzed by gas flow injection – time of flight mass spectrometry (Fuhrer et al., 2011).

Hyperinsulinemic-euglycemic Clamp. Hyperinsulinemic-euglycemic clamps were performed in conscious unrestrained catheterized mice. Seven days prior to the experiment, mice were anesthetized using isoflurane and a silastic catheter (0.012 inch inner diameter) was surgically implanted in the right jugular vein and exteriorized above the neck using vascular access button (Instech Laboratories Inc., Plymouth Meeting, PA). Euglycemic hyperinsulinemic clamps were thus performed in conscious unrestrained catheterized mice. Mice were fasted 5 hr before the start of the experiment (t = 0 min). At t = -120 min, an infusion of [3-^{3}H] glucose (0.05 µCi/min) (Perkin Elmer, Walthman, MA, USA) was initiated. After 120 min, blood samples were collected from the tail vein to measure basal blood glucose and plasma insulin as well as to calculate the rate of endogenous glucose appearance (EndoRa) and glucose disposal (Rd) at basal state. At t = 0 min, a continuous insulin infusion (4 mIU/kg body weight/min.) (NovoRapid, Novo Nordisk Pharma, Zurich, Switzerland) was used to induce hyperinsulinemia. The infusion of [3-^{3}H] glucose was increased to 0.1 µCi/min and 50% glucose was infused to maintain target euglycemia (120 mg/dL) (glucose infusion rate, GIR). At steady state, *in vivo* insulin-stimulated glucose uptake in tissues was determined by a 10 µCi bolus injection of 2-[^{14}C] deoxyglucose (2[^{14}C]DG) (Perkin Elmer). After 30 min, mice were rapidly killed by cervical dislocation and tissues removed and stored at -80°C until use. [3-^{3}H] glucose and 2[^{14}C]DG specific activities were determined in deproteinized blood samples. Plasma insulin was measured by ELISA (Mercodia, Uppsala, Sweden). EndoRa

under insulin stimulated state was determined by subtracting steady state GIR from Rd. Measurements of 2-[^{14}C] deoxyglucose-6-phosphate concentration allowed calculation of the glucose utilization index of individual tissues. These experiments were performed at the Hyperinsulinemic-euglycemic clamp facility of the CMU Geneva, University of Geneva.

Glucose Uptake Under Glucose Stimulated Condition. Glucose uptake in tissues during GTT was measured after intra-peritoneal injection of 2g/kg of D-glucose spiked with 2-[^{14}C] deoxyglucose. After 45 min, mice were sacrificed and tissues rapidly harvested for radioactivity measurement.

Positron Emission Tomography–Computed Tomography (MicroPET-CT). Mice were anesthetized with 2% isoflurane and were injected i.v. with 5-6 MBq of 2-deoxy-2-[^{18}F]fluoro-*D*-glucose ([^{18}F]FDG). Two minutes after injection, mice were PET-scanned for 45 min then subjected to CT in a Triumph microPET/SPECT/CT system (Trifoil, Chatsworth, CA, USA). CT images were obtained at 80 kVp, 160 µA, and 1024 projections were acquired during the 360° rotation with a field of view of 53.1 mm (2.3 × magnification). PET scans were reconstructed as 5 min frames with the built-in LabPET software using an OSEM3D (20 iterations) algorithm and images were calibrated in Bq/mL by scanning a phantom cylinder. The Triumph XO software, which uses a back-projection engine, was used to reconstruct the CT scans with a matrix of 512 and a voxel size of 0.105 mm. CT scans were co-registered with the PET scans using the plugin Vivid (Trifoil) for Amira (FEI, Hillsboro, OR, USA) and exported as dicom files. The software Osirix (Pixmeo, Bernex, Switzerland) was used to quantitatively analyse the datasets and generate pictures. Regions of interest (ROI) were drawn on contiguous slices on CT scans and computed as 3D volumes for the measurements of volumes and densities of indicated adipose tissues. Then, PET series were converted to display Standardised Uptake Values (SUV) adjusted to the body weight of the animals and merged with CT sets. 3D ROIs derived from CT scans were used to quantify the uptake of [^{18}F]FDG in the indicated adipose tissues.

Intestinal Loop. Mucosal to serosal glucose transport was measured as described (Ducroc et al., 2005). Briefly, 30 mM D-glucose spiked with 0.1 µCi/ml D [^{14}C]-glucose (specific activity 55 mCi/mmol) was filled into 2 cm long proximal to mid jejunum segment, ligated at both sides and incubated in KRB buffer at 37°C gassed with Carbogen. Sampling of the bath was performed up to 60 min to assess the glucose transport. At 60 min, intestinal loops were collected, flushed (to collect luminal glucose content) and homogenized (for tissue glucose content) for radioactivity measurements.

RNASeq. Next Gen Sequencing of mRNA transcripts was performed on Ilumina HiSeq 2500 platform at iGE3 facility of the Institute of Genetics and Genomics of Geneva, University of Geneva. RNA was isolated from proximal jejunum segments (n=3 per group, each replicate was a pool of samples from 2 mice), poly-A selected and libraries for sequencing prepared according to Ilumina TrueSeq protocol. The reads were mapped with the TopHat v.2 software to the UCSC mm10 reference; on new junctions and known junctions annotations. Biological quality control and summarization were done with RSeQC-2.3.3 and PicardTools1.92. The differential expression analysis was performed with the statistical analysis R/Bioconductor package EdgeR v. 3.4.2, for the genes annotated in mm10. Briefly, the counts were normalized according to the library size and filtered. The genes having a count above 1 count per million reads (cpm) in at least 3 samples were kept for the analysis. The differentially expressed genes tests were done with a GLM (general linear model) with a negative binomial distribution. The differentially expressed genes p-values are corrected for multiple testing error with a 5%. FDR (false discovery rate). The correction used is Benjamini-Hochberg (BH). For comparison of individual genes (Figure 6), p-value without correction is shown.
For pathway enrichment analysis, transcripts with log(cpm)>1 and $p \leq 0.05$ were selected and multiple comparisons run through MetaCore software pipeline (Thomson Reuters).

TUNEL assay. Terminal deoxynucleotidyl transferase dUTP nick end labeling (TUNEL) assay for detecting DNA fragments (apoptosis) was performed on paraffin-embedded sections of proximal jejunum fixed with 4% PFA with Click-IT TUNEL AlexaFluor647 kit (Invitrogen, C10247), following manufacturer's instructions.

Western Blots. Proximal jejunum segments (~5 mm) were homogenized in RIPA buffer and cleared by centrifugation, according to standard techniques. Western blots of whole tissue lysates were probed with antibodies against: cleaved caspase 3 (1:1000, Cell Signaling #9661), b-actin (1:2000, Cell Signaling, #3700), g-tubulin (1:5000, Sigma Aldrich #T6557), and PCNA (1:2000, Origene #TA800875)

Real Time PCR. 1-2 μg of total RNA was used for cDNA preparation with random hexamer primers using High Capacity cDNA Reverse Transcription kit (Applied Biosystems). Steady-state mRNA expression was measured by quantitative real-time PCR using the LightCycler 480 SYBR Green Master I Mix (Roche) with 386 well LightCycler 480 II (Roche). Transcript levels were normalized to the averaged relative expression of both acidic ribosomal phosphoprotein 36B4 and small ribosomal protein 16 (Rps16) or to beta-2-microglobulin (B2m) for adipose tissue, as indicated. Primer sequences for real-time PCRs were as previously used (Sun and Trajkovski, 2014; Trajkovski et al., 2012) or as given below:

Gene	Forward primer	Reverse primer
Il15	CAGAGGCCAACTGGATAGATG	ACTGTCAGTGTATAAAGTGGTGTCAAT
Bcl2l1	TGACCACCTAGAGCCTTGGA	GCTGCATTGTTCCCGTAGA
Bcl3	GAACAACAGCCTGAACATGG	TCTGAGCGTTCACGTTGG
Mcl1	GGTATTTAAGCTAGGGTCATTTGAA	TGCAGCCCTGACTAAAGGTC
Wnt2b	CCGGGACCACACTGTCTTT	GCTGACGAGATAGCATAGACGA
Vegfa	TTAAACGAACGTACTTGCAGATG	AGAGGTCTGGTTCCCGAAA
Actb	CTAAGGCCAACCGTGAAAAG	ACCAGAGGCATACAGGGACA
Thbs1	CACCTCTCCGGGTTACTGAG	GCAACAGGAACAGGACACCTA
Sgk1	GGACTACATTAATGGTGGAGAGC	CTGGCTATTTCAGCTGCGTA
Slc2a1	GGATCCCAGCAGCAAGAAG	CCAGTGTTATAGCCGAACTGC
Slc2a2	GTCAGCTATTCATCCACATTCAGT	AGCCAAGGTTCCGGTGAT
Slc2a5	AGAGCAACGATGGAGGAAAA	CCAGAGCAAGGACCAATGTC
Slc5a1	CTGGCAGGCCGAAGTATG	TTCCAATGTTACTGGCAAAGAG
B2m	TTGTCTCACTGACCGGCCT	TATGTTCGGCTTCCCATTCTCC
Rps16	GGCTCATCAAGGTGAACGGA	AAATCGCTCCTTGCCCAGAA

Caloric Uptake. Mice were housed 2 per cage, and food intake and feces production were measured and collected per 24 hr. The feces were dried and ground to a fine powder before subjecting them to an oxygen bomb calorimeter (Parr, 6100, USA) according to the manufacturer's instructions. Calorie excretion was calculated by multiplying the produced feces with the calories content per gram of feces. Calorie uptake was calculated by subtracting caloric content of the feces from the caloric content in consumed food per 24h.

Energy Expenditure. Energy expenditure between day 3 and day 21 after microbiota transplantation was calculated as described (Ravussin et al., 2013) (Guo and Hall, 2011) using the following formula:

$$Energy\ expenditure\ \left(\frac{kcal}{g}\right) = Energy\ intake\ \left(\frac{kcal}{g}\right) - 9.4\frac{kcal}{g} * \Delta fat\ mass + 1.8\frac{kcal}{g} * \Delta fat\ free\ mass$$

Energy intake was calculated by multiplying the weight of the food consumed from day 3 to 21 by the caloric content (3.64 kcal/g), assuming equal consumption by two cage mates. Fat mass difference was calculated from CT quantification of subcutaneous and visceral fat depots at day 3 and day 21. Fat-free mass difference was calculated from initial and end body weights minus quantified fat. 9.4 and 1.8 kcal/g are empirical values for energy content of fat and lean mass (Guo and Hall, 2011).

Intestinal Transit Time. Mice were gavaged at 8:00 a.m. with suspension of 6% carmine red (Sigma) in 0.5% methylcellulose (Sigma, M0262), placed in single cages without access to food, then monitored every 5 min as shown previously (Menacho-Marquez et al., 2013). Time of the appearance of red stool was recorded as a total transit time.

Histology and Immunofluorescence. Tissues were extracted, fixed in 4% paraformaldehyde (Sigma), paraffin embedded, cut in 5µm thick sections and stained with hematoxylin-eosin (H&E) using standard techniques. Goblet cells were stained with Alcian blue (MERK) and counterstained with Nuclear Fast Red. Immunohistochemistry

were done using rabbit anti-UCP1 (Pierce PA1-24894, 1:100), goat anti-LysosymeC (Santa Cruz sc-27958, 1:100) and goat anti Chromogranin A (Santa Cruz sc-1488, 1:100). Anti-rabbit Cy3 (Jackson 711165152, 1:250), anti-goat FITC (Life technologies A16006, 1:500) and anti-goat-HRP (Life technologies A15999, 1:500) were used as secondary antibodies. Probes used for in- situ hybridization targeting olfm4 were synthetized by *in vitro* transcription with an RNA labeling kit (Roche) from a PCR DNA template generated using the forward mmu-Olfm4_T7 (5'CCG**TAATACGACT CACTATAGGG**AACATCACCCCAGGCTACAG 3') and the reverse mmu-Olfm4_SP6 (5'CCG**ATTTAGGTGACACTATAGAA**GCCAGTTGAGCTGAATCAC A 3') primers from cDNA obtained from mouse jejunum RNA extract. Images were acquired using Mirax (Zeiss) slide scanner microscope. Intestine morphometry was measured with Panoramic viewer (3D Histech), Paneth, enteroendocrine, goblet and Lgr5+ stem cells were quantified using Definiens Developer XD2 software, and cell/lipid droplet size quantification was performed using MetaMorph software (V7.7.6.0, Molecular Devices). All light microscopy and quantifications was done at Bioimaging Core Facility of Faculty of Medicine, University of Geneva.

Electron microscopy (EM): After sacrifice, jejunum samples were fixed by immersion in a 2.5% glutaraldehyde solution (Sigma), post-fixed in 2% osmium tetroxide, stained en block with uranyl acetate and dehydrated and embedded in Epon 812 (Fluka Chemie, Buchs, Switzerland). Thin sections were cut and stained with uranyl and lead citrate. Images were obtained using Morgagni microscope (FEI Company, Eindhoven, Netherlands). EM was done at EM Core Facility of Faculty of Medicine, University of Geneva

Statistical Analysis. Unless otherwise specified in the figure legends, significance was calculated using non-paired two-tailed Student's t-test.*: $p \leq 0.05$, **: $p \leq 0.01$, ***: $p \leq 0.001$, Brackets [ ] show significance between all pairs in the dataset. All values show mean ± sd, unless specified. All experiments were performed at least three times, and the representative experiment is shown. Sample sizes and animal numbers were chosen based on power calculations of 0.8.

2) Supplemental Tables

Metabolite [a]	RT		RT+Abx		Cold (6°C)		Cold+Abx		t-test (p-values) [b]		
	Mean	SD	Mean	SD	Mean	SD	Mean	SD	RT vs RT+Abx	6C vs 6C+Abx	RT vs Cold
PLASMA											
Acetone	14252	1237	11067	1764	13403	1691	11182	1212	**0.0009**	**0.0129**	0.2709
Acetate	51076	4882	40687	4701	51591	4706	43369	4115	**0.0007**	**0.0034**	0.8330
Pyruvate	67462	8127	70993	9250	65093	6840	63809	6256	0.4308	0.7121	0.5385
Propionate	12351	823	12108	1540	13391	476	12962	1077	0.7001	0.3251	**0.0080**
Butyrate	7856	838	7949	535	8743	1196	8043	286	0.7963	0.1563	0.1078
Lactate	2926356	919692	2487622	491913	1694495	237921	1753791	546391	0.2539	0.7844	**0.0025**
Acetoacetate	42948	3099	37632	2523	43429	5046	38206	4676	**0.0021**	0.0591	0.8218
Hydroxybutyrate	70857	19156	61196	11542	137505	59524	119296	36631	0.2420	0.4964	**0.0093**
Fumarate	9697	2156	13582	5817	15033	6709	13055	6712	0.0983	0.5787	**0.0503**
Succinate	8781	1624	9808	4022	10286	1559	10303	1822	0.5142	0.9847	0.0796
CECUM											
Acetone	10041	1465	13724	1653	8930	1693	14146	700	**0.0003**	**0.0000**	0.1823
Acetate	22216	2938	32557	4090	22414	3268	36280	1554	**0.0000**	**0.0000**	0.9003
Pyruvate	44706	3627	85363	15937	44777	5026	90872	6047	**0.0000**	**0.0000**	0.9749
Propionate	12690	1213	19684	3453	11129	1250	22704	944	**0.0001**	**0.0000**	**0.0238**
Butyrate	239212	79243	4770	725	262692	101515	5300	775	**0.0000**	**0.0000**	0.6141
Lactate	309546	129673	226861	108164	185599	109860	192868	56932	0.1877	0.8776	0.0582
Acetoacetate	28412	1885	84358	24715	33685	7384	95822	5117	**0.0000**	**0.0000**	0.0706
Hydroxybutyrate	11611	4305	9278	1839	13062	4436	12048	1286	0.1806	0.5708	0.5174
Fumarate	8083	2486	6192	1303	7340	3616	5551	788	0.0775	0.2240	0.6396
Succinate	95436	24099	28043	20962	91668	19589	18227	3484	**0.0000**	**0.0000**	0.7366

Table S1. Relative Quantities of Short-Chain Fatty Acids (SCFA) in Plasma and Cecum

SCFA levels in plasma and cecum samples of RT or cold exposed mice with or without Abx for 30 days after 5 hr fasting (n=8 per group).

[a] Ion intensities (arbitrary values)

[b] p-values rounded to 4 decimal places, significant ($p \leq 0.05$) differences are in bold

Metabolite [a]	Germ-free		RT transplanted		Cold transplanted		t-test (p-values) [b]		
	Mean	SD	Mean	SD	Mean	SD	GF:RT trans	GF:Cold trans	RT tr: Cold tr
PLASMA									
Acetone	8017	1311	8332	751	8840	877	0.6184	0.2198	0.2534
Acetate	32939	5154	34811	2843	35186	3888	0.4490	0.4143	0.8369
Pyruvate	49582	6188	44995	4108	49911	3743	0.1695	0.9096	**0.0306**
Propionate	11781	1095	12128	1067	12059	581	0.6194	0.5697	0.8764
Butyrate	7033	324	6871	490	6876	243	0.5725	0.3641	0.9796
Lactate	1022758	333852	980672	271659	1192952	213612	0.8244	0.3026	0.1141
Acetoacetate	26023	2083	24255	693	25660	2216	0.0629	0.7913	0.1327
Hydroxybutyrate	26171	3756	55827	42990	59993	37190	0.2114	0.1069	0.8435
Fumarate	8038	915	7875	690	7980	771	0.7442	0.9102	0.7869
Succinate	9327	1186	8886	923	10224	1458	0.5073	0.3138	0.0573
CECUM									
Acetone	12381	547	5216	706	5312	892	**0.0000**	**0.0000**	0.7474
Acetate	36729	3730	19655	2369	21573	3439	**0.0000**	**0.0000**	0.0906
Pyruvate	118652	9047	39654	3659	40517	4020	**0.0000**	**0.0000**	0.5457
Propionate	15359	2005	11490	1082	13406	1899	**0.0000**	**0.0468**	**0.0025**
Butyrate	43678	58858	256218	62775	346505	150430	**0.0000**	**0.0001**	**0.0460**
Lactate	2719683	492114	64981	20877	85786	21845	**0.0000**	**0.0000**	**0.0129**
Acetoacetate	91450	8186	24569	2876	26767	4785	**0.0000**	**0.0000**	0.1458
Hydroxybutyrate	76792	18202	4849	1391	5874	2031	**0.0000**	**0.0000**	0.1232
Fumarate	5414	582	4998	4459	5251	2615	0.8251	0.8831	0.8487
Succinate	21421	2992	88137	50114	154989	80349	**0.0049**	**0.0007**	**0.0120**

Table S2. Relative Quantities of SCFA in Plasma and Cecum

SCFA levels in plasma or cecum of GF (n=4), RT (n=8) or cold (n=8) transplanted mice (day 21) after 5 hr fasting.

All values in Tables S1 and S2 show mean ± sd. Significance was calculated using non-paired two tailed Student's t-test.*: $p \leq 0.05$, **: $p \leq 0.01$, ***: $p \leq 0.001$.

[a] Ion intensities (arbitrary values)

[b] p-values rounded to 4 decimal places, significant ($p \leq 0.05$) differences are in bold

Amplification region		Primer sequence	References
16SrRNA V2-V3 region	*Forward*	AGAGTTTGATCCTGGCTCAG	(Haakensen et al., 2008; Hermann-Bank et al., 2013; Liu et al., 2008; Muhling et al., 2008; Schwieger and Tebbe, 1998)
	Reverse	CTGCTGCCTYCCGTA	
16SrRNA V4-V5 region	*Forward*	CAGCAGCCGCGGTAATAC	(Haakensen et al., 2008; Hermann-Bank et al., 2013; Muhling et al., 2008; Schwieger and Tebbe, 1998)
	Reverse	CCGTCAATTCCTTTGAGTTT	
Phylum Firmicutes 16S region	*Forward*	CTGATGGAGCAACGCCGCGT	(Haakensen et al., 2008; Hermann-Bank et al., 2013; Muhling et al., 2008)
	Reverse	ACACYTAGYACTCATCGTTT	
Phylum Bacteroidetes 16S region	*Forward*	CCGGAWTYATTGGGTTTAAAGGG	(Hermann-Bank et al., 2013; Muhling et al., 2008)
	Reverse	GGTAAGGTTCCTCGCGTA	
Akkermancia Muciniphila 16S region	*Forward*	CAGCACGTGAAGGTGGGGAC	(Everard et al., 2013)
	Reverse	CCTTGCGGTTGGCTTCAGAT	

Table S3. Primer Sequences Used for Gut Microbiota Profiling by qPCR

3) Supplemental References

Derrien, M., Collado, M.C., Ben-Amor, K., Salminen, S., and de Vos, W.M. (2008). The mucin degrader Akkermansia muciniphila is an abundant resident of the human intestinal tract. Appl Environ Microb *74*, 1646-1648.

Ducroc, R., Guilmeau, S., Akasbi, K., Devaud, H., Buyse, M., and Bado, A. (2005). Luminal leptin induces rapid inhibition of active intestinal absorption of glucose mediated by sodium-glucose cotransporter 1. Diabetes *54*, 348-354.

Everard, A., Belzer, C., Geurts, L., Ouwerkerk, J.P., Druart, C., Bindels, L.B., Guiot, Y., Derrien, M., Muccioli, G.G., Delzenne, N.M.*, et al.* (2013). Cross-talk between Akkermansia muciniphila and intestinal epithelium controls diet-induced obesity. Proceedings of the National Academy of Sciences of the United States of America *110*, 9066-9071.

Fiehn, O., and Kind, T. (2007). Metabolite profiling in blood plasma. Methods in molecular biology *358*, 3-17.

Fuhrer, T., Heer, D., Begemann, B., and Zamboni, N. (2011). High-throughput, accurate mass metabolome profiling of cellular extracts by flow injection-time-of-flight mass spectrometry. Analytical chemistry *83*, 7074-7080.

Grivennikov, S.I., Wang, K., Mucida, D., Stewart, C.A., Schnabl, B., Jauch, D., Taniguchi, K., Yu, G.Y., Osterreicher, C.H., Hung, K.E*., et al.* (2012). Adenoma-linked barrier defects and microbial products drive IL-23/IL-17-mediated tumour growth. Nature *491*, 254-258.
Guo, J., and Hall, K.D. (2011). Predicting changes of body weight, body fat, energy expenditure and metabolic fuel selection in C57BL/6 mice. PloS one *6*, e15961.
Haakensen, M., Dobson, C.M., Deneer, H., and Ziola, B. (2008). Real-time PCR detection of bacteria belonging to the Firmicutes Phylum. International journal of food microbiology *125*, 236-241.
Hermann-Bank, M.L., Skovgaard, K., Stockmarr, A., Larsen, N., and Molbak, L. (2013). The Gut Microbiotassay: a high-throughput qPCR approach combinable with next generation sequencing to study gut microbial diversity. BMC genomics *14*, 788.
Liu, Z., DeSantis, T.Z., Andersen, G.L., and Knight, R. (2008). Accurate taxonomy assignments from 16S rRNA sequences produced by highly parallel pyrosequencers. Nucleic acids research *36*, e120.
Menacho-Marquez, M., Nogueiras, R., Fabbiano, S., Sauzeau, V., Al-Massadi, O., Dieguez, C., and Bustelo, X.R. (2013). Chronic sympathoexcitation through loss of Vav3, a Rac1 activator, results in divergent effects on metabolic syndrome and obesity depending on diet. Cell metabolism *18*, 199-211.
Muhling, M., Woolven-Allen, J., Murrell, J.C., and Joint, I. (2008). Improved group-specific PCR primers for denaturing gradient gel electrophoresis analysis of the genetic diversity of complex microbial communities. The ISME journal *2*, 379-392.
Ravussin, Y., Gutman, R., LeDuc, C.A., and Leibel, R.L. (2013). Estimating energy expenditure in mice using an energy balance technique. International journal of obesity *37*, 399-403.
Schwieger, F., and Tebbe, C.C. (1998). A new approach to utilize PCR-single-strand-conformation polymorphism for 16S rRNA gene-based microbial community analysis. Applied and environmental microbiology *64*, 4870-4876.
Sun, L., and Trajkovski, M. (2014). MiR-27 orchestrates the transcriptional regulation of brown adipogenesis. Metabolism *63*, 272-282.
Trajkovski, M., Ahmed, K., Esau, C.C., and Stoffel, M. (2012). MyomiR-133 regulates brown fat differentiation through Prdm16. Nat Cell Biol *14*, 1330-1335.

Supplemental Figure Legends

Figure S1: Body Weight and Temperature After Cold Exposure and Antibiotics (Abx) Treatment, Related to Figure 1

(A, B) Body weight gain (A), and food consumption (B) of cold exposed mice and RT controls over 36 days.

(C, D) Weight of ingSAT (C), and pgVAT (D) of cold exposed mice and RT controls for 10 (n=4 per group), or 31 days.

(E) Ratios of cold vs. RT fat amount at days 10 and 31 shown as % of mice as in (C, D)

(F) Resting energy expenditure (REE) in RT or cold exposed mice, measured between day 0 and day 31 after cold exposure, shown per day.

(G) Calorimetric measurements of 24hr fecal caloric content of Abx or control mice (n=8 per group). Mice were kept 2 per cage. Each cage was considered as one pooled sample (n=4).

(H-J) Body weight (H), changes in body weight relative to start value (I) and blood glucose levels (J) of mice with or without access to food exposed to cold for 4 and 8 hr (see Figure 1A for associated body temperature).

(K-N) Rectal body temperature of Abx and control mice after 3, 6 and 12 hr of acute cold exposure, performed at week 1 (K), week 2 (L), weeks 3 (M), and week 4 (N) after the start of the Abx treatment.

(O-R) Blood glucose of mice as in (K-N, respectively) performed at week 1 (O), week 2 (P), weeks 3 (Q), and week 4 (R) after the start of the Abx treatment.

(S, T) Food intake (S), and water consumption (T) during cold exposure of mice as in (K-N). The shown amount is for the total period of cold exposure.

All panels show mean ± sd, except K-R, which show mean ± sem. Unless otherwise stated, in all panels n=8 per group. Significance was calculated using non-paired two-tailed Student's t-test.*: $p \leq 0.05$, **: $p \leq 0.01$, ***: $p \leq 0.001$.

Figure S2. Cold Exposure Induces Major Reshaping of the Gut Microbiota, Related to Figure 1

(A-B) PCoA based on Weighted UniFrac analysis on operational taxonomic units (OTUs). Each symbol represents a single sample of cecum content of 31 days cold exposed mice (n=5) and their RT controls (A) (n=4); and of feces after 0, 11 and 31 days of cold exposure (B) (n=6-7 per group).

(C, E) Phylum level proportional abundance as described in the barchart of Figure 1G in (C) feces (n=7+8) and (E) cecum (n=4+5).

(D, F) Hierarchical clustering diagram constructed using the average-neighbor (HC-AN) method comparing (D) cecum content (n=4-5 per group) and (F) feces sample (n=7-8 per group) of 31 days cold or RT exposed mice. The heat map shows the relative abundance of the top 100 OTUs displaying the most significant p-value after a Welch t-test comparison of the two groups. The assigned OTUs are presented as the following: Phylum, Class, Order, Family, Genus, and Specie. R: RT; C: Cold exposed; with suffix c: cecum; without suffix: feces.

All values show mean ± sd. Significance was calculated using non-paired two-tailed Student's t-test.*: $p \leq 0.05$, **: $p \leq 0.01$, ***: $p \leq 0.001$.

Figure S3. Cold Exposure Alters the Gut Microbiota and Abolishes *A. muciniphila*, Related to Figure 1

(A, B) Hierarchical clustering diagram constructed using the average-neighbor (HC-AN) method comparing cecum (n=4-5 per group) and feces (n=6-7) of 31-day cold or RT exposed mice. In (A) associated heat map shows the relative abundance of the top 100 OTUs displaying the most significant p-value after a Welch t-test comparison of the two groups. In (B) associated heat map shows the relative abundance of representative OTUs selected for a chosen p-value threshold ($p < 0.05$), obtained with a Welch t-test comparison of the two groups, and then grouped into families. One representative OTU with the greatest difference between the two group means from each family is selected for inclusion in the heat map diagram. R: RT; C: Cold exposed; with suffix c: cecum; without suffix: feces.

(C, D) Bacterial diversity assessed by Shannon diversity index of feces (C) collected after 0, 11 or 31 days of cold exposure and their RT controls and cecum content (D) of 31-day cold or RT exposed mice (n=4-5 per group).

(E, F) *Akkermansia muciniphila* species abundance in feces (E) (n=6+8), and cecum content (F) (n=4+5) of 31-day cold or RT exposed mice assessed by 16S sequencing.

(G, H) Profiles of the top 9 OTUs generating the lowest p-value after ANOVA analysis when comparing (G) cecum content (n=4+5) and (H) feces (n=6+8) of 31-day cold exposed and RT control mice. The y-axis represents the OTU abundance.

(I, J) Relative abundance of Firmicutes (I) and Bacteroidetes (J) phylum in 31-day cold exposed mice and RT controls kept in conventional animal facility, quantified by qPCR and normalized to bacteria universal 16SrRNA (V4-V5 region) (n=8 per group).

(K, L) Relative abundance of Firmicutes (K) and Bacteroidetes (L) phylum in mice transplanted with RT or cold microbiota at day 19 after colonization (n=6-7 per group); and their donors kept in SPF conditions at the day of colonization (n=6 per group), quantified by qPCR and normalized to bacteria universal 16SrRNA (V4-V5 region).

Unless otherwise stated, all values show mean ± sd. Significance was calculated using non-paired two-tailed Student's t-test.*: $p \leq 0.05$, **: $p \leq 0.01$, ***: $p \leq 0.001$.

Figure S4. Increased Glucose Peak During OGTT and Increased Insulin Sensitivity of Cold Exposed Mice With or Without Microbiota Depletion, Related to Figure 2, Figure 3 and Figure 5

(A) Steady-state glucose infusion rate (GIR) in RT and cold-exposed mice during euglycemic-hyperinsulinemic clamp (n=6).

(B) Coronal view of the CT scans of cold or RT transplanted mice 21 days after transplantation.

(C-G) Normalized (C, E, G), or absolute (D, F) glucose levels during OGTT of RT or cold exposed male mice with or without Abx at day 23 (C) and day 7 (D, E); or female mice at day 16 (F, G) (n=4 per group).

(H, I) Insulin tolerance test (ITT) at day 8 (H) and intra-peritoneal glucose tolerance test (IPGTT) at day 17 (I) of RT or cold exposed male mice with or without Abx (n=8 per group).

(J) Insulin levels during OGTT as in Figure 5B of RT or cold transplanted mice (n=6 per group).

All values show mean ± sd. Significance was calculated using non-paired two-tailed Student's t-test.*: p≤0.05, **: p≤0.01, ***: p≤0.001

Figure S5. Cold Exposure and Abx Treatment Increase Small Intestinal Length and Weight, Related to Figure 5

(A) Images of representative RT or cold exposed male mice with or without antibiotics during dissection at day 31.

(B, C) Small intestine length (B) and weight (C) of RT or cold exposed mice with or without antibiotics (day 9) (n=4 per group).

(D) Weights of different organs of gastrointestinal tract of mice as in (A) (n=8 per group).

(E-G) Weights of different organs of gastrointestinal tract (E), Fat pads (F), or other organs (G) collected from of RT or cold exposed GF mice (n=6 per group).

(H) Weights of different organs of gastrointestinal tract of GF, RT or cold transplanted mice at day 21 after transplantation (GF n=4, RT and Cold transplanted n=8 per group).

All values show mean ± sd. Significance was calculated using non-paired two-tailed Student's t-test.*: p≤0.05, **: p≤0.01, ***: p≤0.001.

Figure S6. Changes in the Intestinal Cell Composition, Related to Figure 6

(A) Immunofluorescence of chromogranin A in ileum sections of RT or cold exposed mice with or without antibiotics (day 31).

(B, C) Total number of chromogranin A positive cells per section (B) or relative proportion of chromogranin A positive cells per tissue surface (C) of sections as in (A) (n=5 per group).

(D) Immunofluorescence of chromogranin A in duodenum sections of RT or cold microbiota transplanted female mice (day 19 post transplantation).

(E) Relative proportion of chromogranin A positive cells per tissue surface (C) of sections as in (D) (n=5 per group).

(F) Alcian blue staining (for goblet cells) of duodenum sections of RT or cold exposed mice with or without Abx (day 31).

(G, H) Total number of goblet cells per section (G) and relative proportion of goblet cells normalized to perimeter (H) of sections as in (F) (n=6 per group).

(I) *In situ* hybridization for Olfm4 of duodenum sections of RT or cold exposed mice with or without antibiotics (day 31).

(J, K) Quantification of total number of Olfm4+ cells per section (J) and relative proportion of Olfm4+ cells normalized to perimeter (K) of sections as in (I) (n=6 per group).

(L) Alcian blue staining for goblet cells of duodenum sections of RT or cold microbiota transplanted female mice (Day 19 post transplantation).

(M) Total number of goblet cells per section of duodenum as in (L) (n=6 per group).

(N) Heatmap of $\log_2$ fold change of gene expression from most significantly regulated patways of mice as in (A), compared to RT=1. Each value represents pooled sample from two mice.

All values show mean ± sd. Significance was calculated using non-paired two-tailed Student's t-test.*: $p \leq 0.05$, **: $p \leq 0.01$, ***: $p \leq 0.001$.

Figure S7. *A. muciniphila* Supplementation Over Cold Microbiota Reduces Intestinal Length But Does Not Affect the Browning, Related to Figure 7

(A) Representative images of cecum, small and large intestine of mice transplanted with cold microbiota with or without *A. muciniphila* co-transplantation.

(B) Insulin levels during OGTT as in Figure 7F of mice transplanted with cold microbiota with or without *A. muciniphila* co-transplantation (n=6 per group, day 23).

(C) Insulin tolerance test normalized to initial glycemia of mice as in (A) (n=6 per group, day 16).

(D) Relative mRNA expression in ingSAT tissues 5 weeks after transplantation of mice as in (A) quantified by real-time PCR and normalized to the house keeping beta-2-microglobulin (*B2m*) *Rplp0* (36b4) and *Rsp16* (n=6 per group).

(E-G) Infrared temperature readings of eye (E), ventral (F) or dorsal (G) temperature after 4 hr cold exposure (day 18).

(H-J) Infrared temperature readings of eye (H), ventral (I) or dorsal (J) temperature after 12 hr cold exposure (day 18).

(K, L) Relative abundance of Bacteroidetes (K) and Firmicutes (L) phylum in mice transplanted with RT or cold microbiota with or without *A.muciniphila* 21 days after transplantation, quantified by qPCR and normalized to bacterial universal 16SrRNA (V4-V5 region). In (E-L) n=10 cold transplanted, n=6 cold co-transplanted with *A.muciniphila*.

(M-P) (M) Bacterial abundance per g of feces (day 10), (N) intestinal length, (O) duodenum perimeter, and (P) distribution of microvilli lengths from EM images from GF mice monocolonized with *A.muciniphila* at 7 weeks of age and kept at RT for 12 days (n=4 per group).

(Q, R) (Q) Body weight, and (R) fat pad weight of cold exposed 7 weeks old C57BL6J mice, exposed to cold for 7 days and gavaged daily with fresh *A.muciniphila* monoculture resuspended in anaerobic PBS or by vehicle (PBS).

(S) Food consumption of mice as in (P). Values show the food intake of 2 mice per 24 hrs.

(T) Relative bacterial abundance of mice as in (Q) 7 days after the start of treatment, quantified by qPCR and normalized to bacteria universal 16SrRNA (V4-V5 region).

(U) Area under the curve during the first 30 min of OGTT as in Figure 7I of mice as in (Q) day 6 days after the start of treatment.

In (Q-R) n=5 per group. All values show mean ± sd. Significance was calculated using non-paired two tailed Student's t-test.*: $p \leq 0.05$, **: $p \leq 0.01$, ***: $p \leq 0.001$.

Figure S1

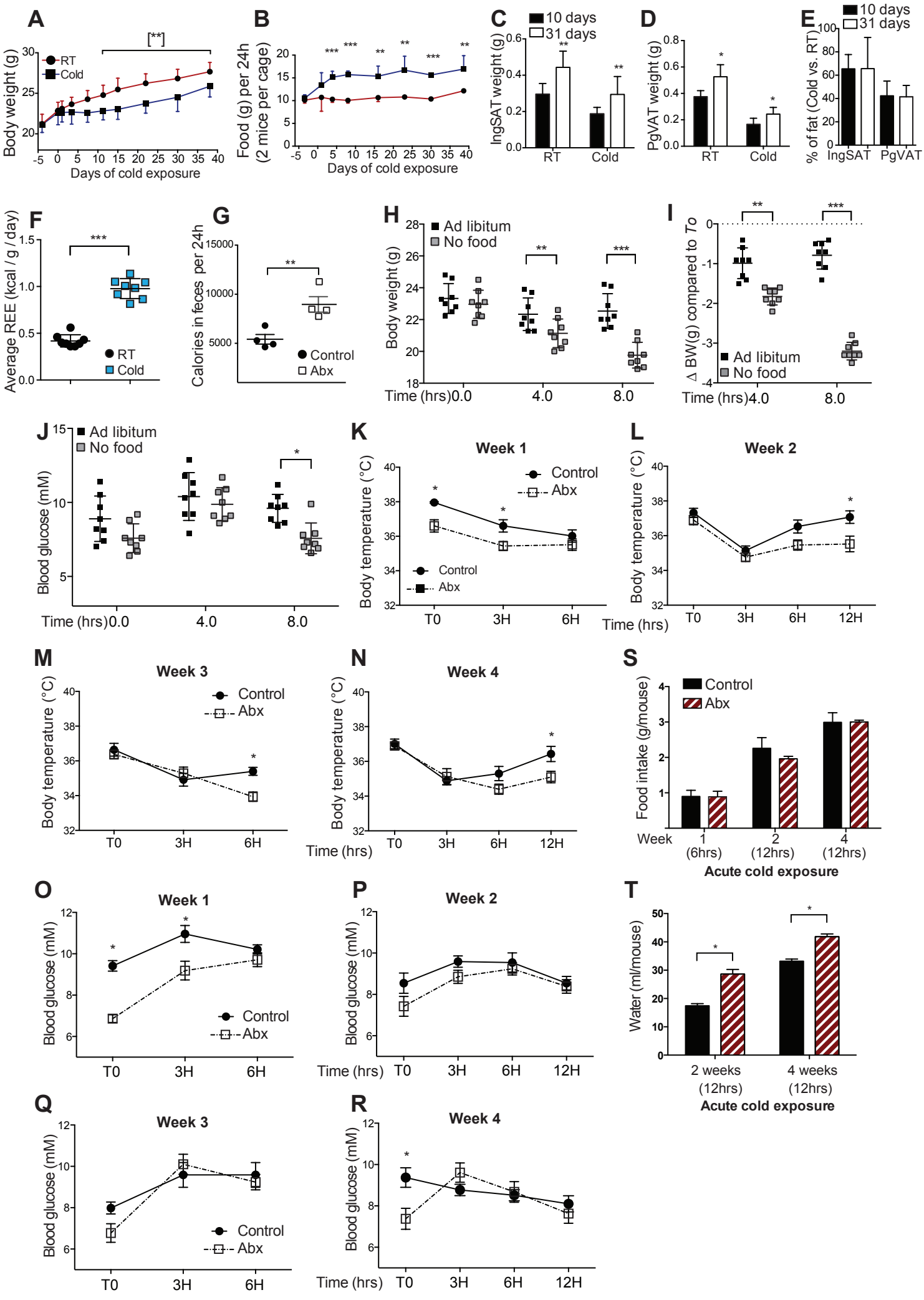

Figure S2

Click here to download Supplemental Figure Supplementary_Figure_2.pdf

Figure S2

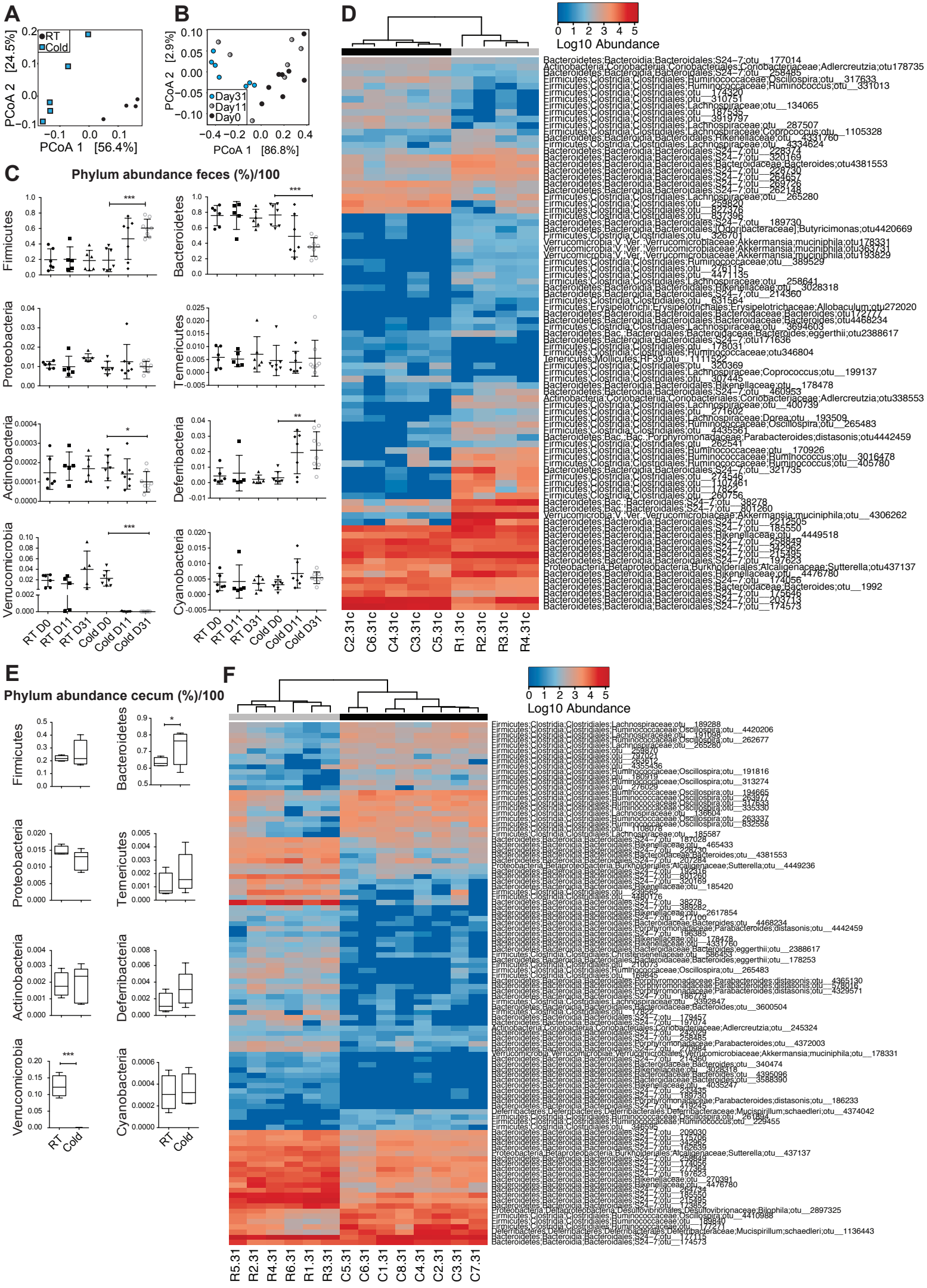

Figure S3

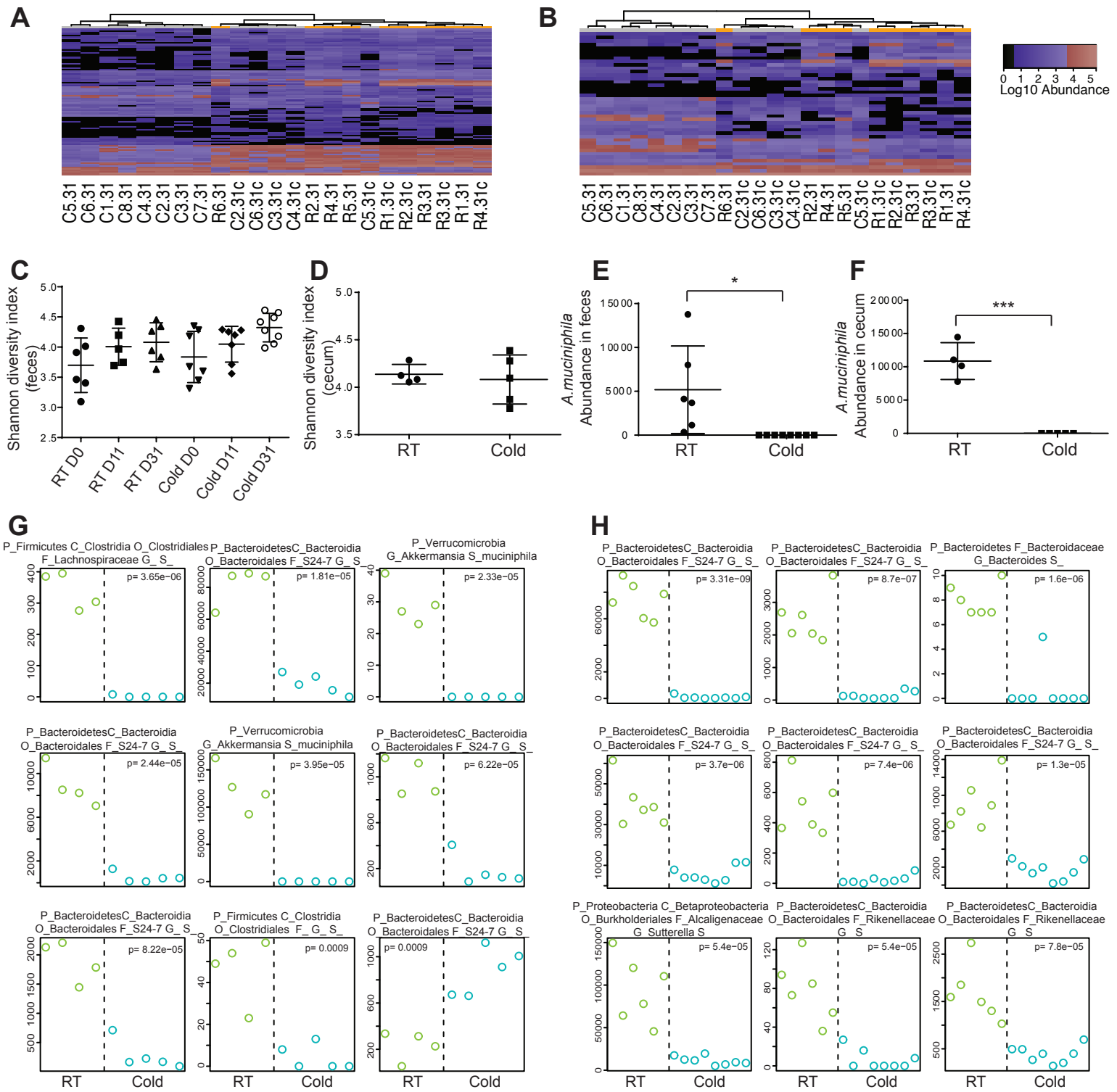

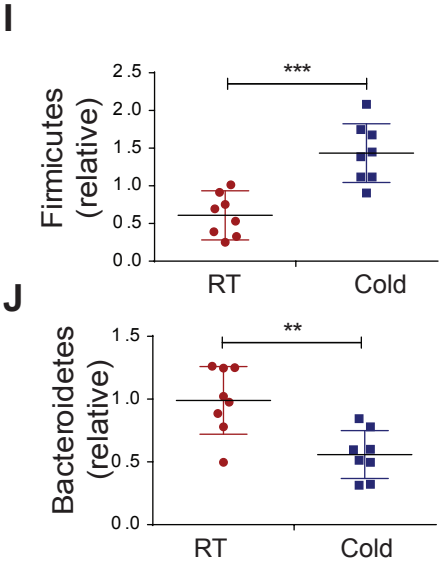

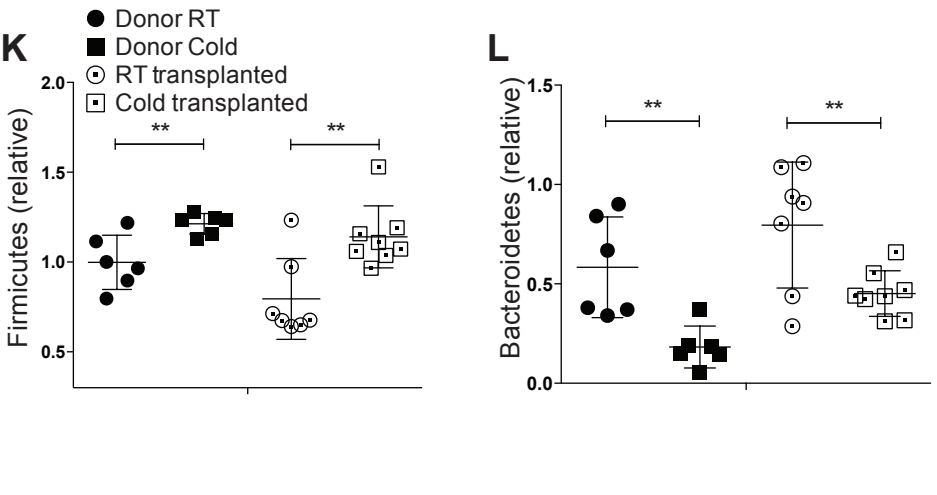

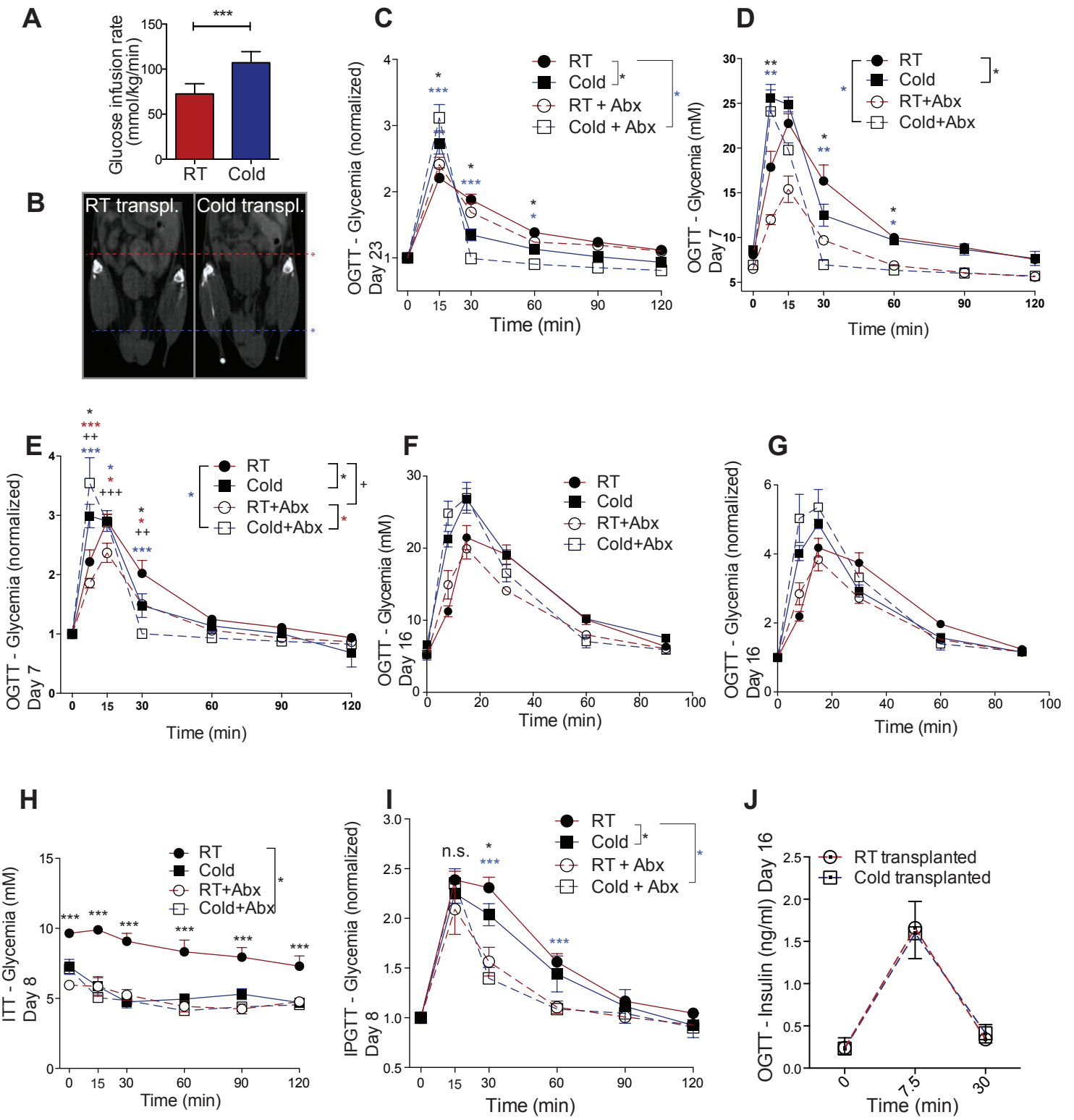

Click here to download Supplemental Figure Supplementary_Figure_5.pdf

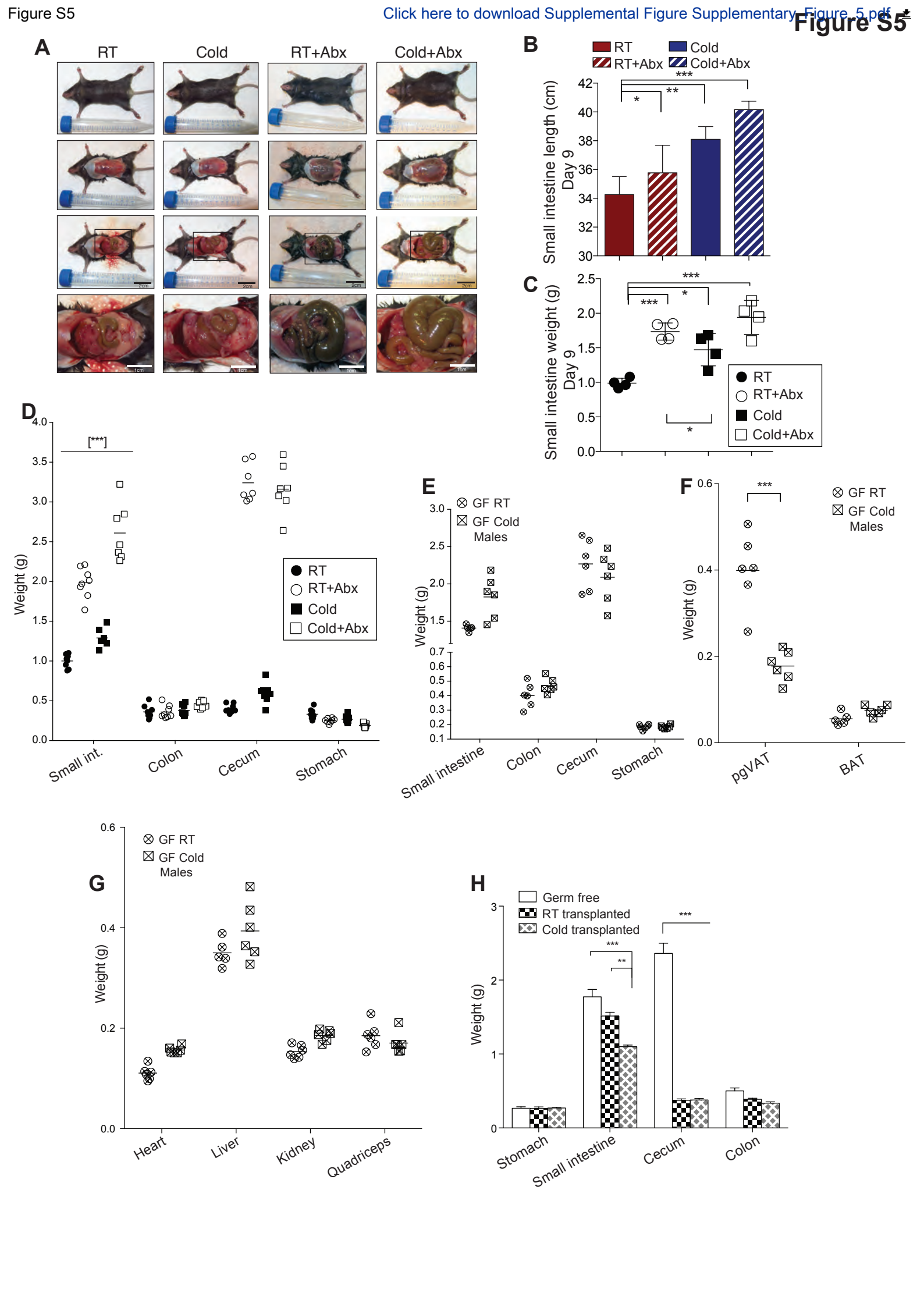

Figure S6

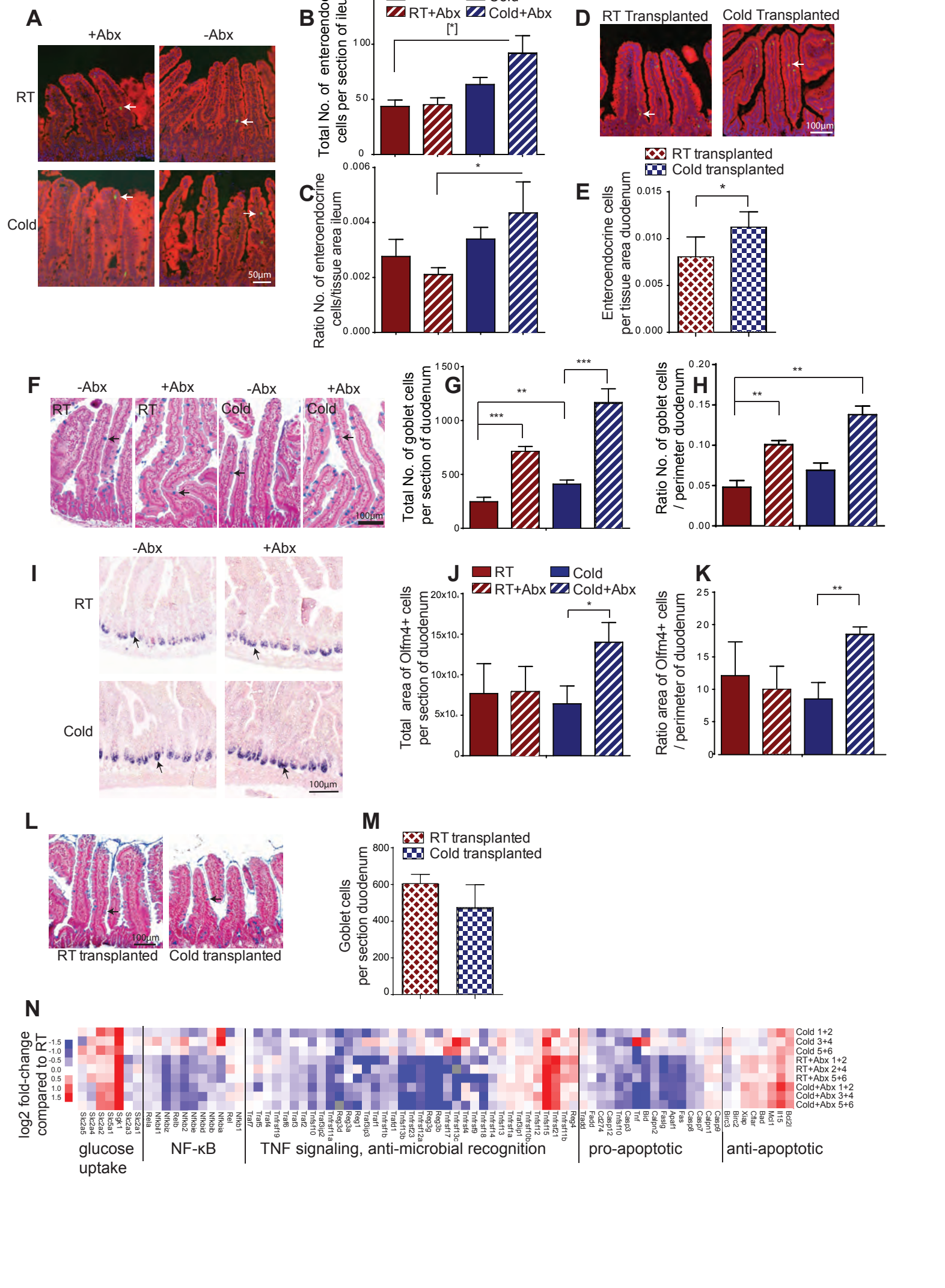

Figure S7